Assessing spatial variation and reflectance of ground calibration targets

Kwame Botchway

March, 2011

Course Title: Geo-Information Science and Earth Observation
                         for Environmental Modelling and Management

Level: Master of Science (MSc)

Course Duration: September 2009 – March 2011

Consortium partners: University of Southampton (UK)
                         Lund University (Sweden)
                         University of Warsaw (Poland)
                         University of Twente, Faculty ITC (The Netherlands)

Assessing spatial variation and reflectance of ground calibration targets
By

Kwame Botchway

Thesis submitted to the University of Twente, faculty ITC, in partial fulfilment of the requirements for the degree of Master of Science in Geo-information Science and Earth Observation for Environmental Modelling and Management

Thesis Assessment Board

Chair: **Prof. Dr. Ir. Alfred Stein**
Internal Examiner: **Prof. Dr. Ing. Wouter Verhoef**
External Examiner: **Dr**. **Jadunandan Dash**
First Supervisor: **Dr. Nicholas Hamm**
Second Supervisor: **Prof. Edward Milton**

Abstract

Ground calibration targets (GCTs) are useful in characterizing the radiometric quality of satellite sensors via vicarious calibration (VC) campaigns. However, these targets are always assumed to be spatially homogeneous. A well-characterized GCT with regards to its spatial homogeneity and temporal stability properties is crucial to the quantification of errors/uncertainties associated with satellite sensors post-launch. Radiometric calibration errors are transferrable throughout the lifespan of a sensor and can generate uncertainties in the sensor's derived products, compromising the evidence base for decision making. This study sought to identify and investigate "spatial homogeneity" property of GCTs for a thorough understanding of their spatial structure. The study further aims at characterising the influence of scale (pixel size and window size) measurements on spatial homogeneity property of GCTs assessment.

This study developed and tested a framework to characterize homogeneity property of GCTs based on Spatial Homogeneity Criteria (SHC) which combines $Gi^* > 0$ and $CV < 3\%$ within a localised 3×3 window and variogram/correlogram to characterize the spatial structure of Tuz Gölü test site. These were geared towards establishing best practice guidelines for VC campaigns. Local variation in HDRF across the VNIR and SWIR bands were evaluated for a proposed VC site in Tuz Gölü, Turkey from fine to coarse resolutions using Landsat TM, MODIS multi-temporal imagery and one ASTER image.

An area that was spatially homogeneous, temporally stable and exhibited normal distribution in the Landsat TM VNIR spectra (approximately 1400 m × 800 m) was identified as a proposed VC site in Tuz Gölü, Turkey. Identification of such an area across the Landsat TM SWIR bands was not possible due to high variation in the observed CV computation attributable to the geomorphologic properties of the site. It was found that the SHC identified areas within a localised 3×3 window tends to decrease from fine to coarse resolution across the VNIR and SWIR bands, possibly due to the observed increment in CV computation from fine to coarse resolution. This study provides knowledge on the characterization of the spatial variation and reflectance (HDRF) of GCTs respecting their spatial homogeneity property and has implication on the use GCTs for VC and more widely, for their use in atmospheric correction (Bannari et al., 2005; Kneubühler et al., 2006).

Keywords: Uncertainty, Hemispherical Directional Reflectance Factor (HDRF), Ground Calibration Targets (GCTs).

Acknowledgements

Table of contents

List of figures

List of tables

List of Appendices

List of abbreviations

AC	Atmospheric correction
AOT	Aerosol Optical Thickness
ASTER	Along Track Scanning Radiometer
BRDF	Bidirectional Distribution Reflectance Function
CEOS	Committee on Earth Observation Satellites
CV	Coefficient of variation
GCTs	Ground Calibration Targets
HDRF	Hemispherical Directional Reflectance Function
HCRF	Hemispherical Conical Reflectance Function
IFOV	Instantaneous Field of View
LPDAAC	Land Processes Distributed Active Archive Centre
MODIS	Moderate Resolution Imaging Spectro-radiometer
NCAVEO	Network for Calibration and Validation of EO data
NPL	National Physics Laboratory
SAA	Solar Azimuth Angle
SHC	Spatial Homogeneity Criteria
SPOT	Satellite Pour l'Observation de la Terre
SZA	Solar Zenith Angle
SWIR	Shortwave Infrared
TG	Tuz Gölü
TOA	Top of Atmosphere
VC	Vicarious calibration
VNIR	Visible and Near Infrared
WGCV	Working Group on Calibration and Validation

1.   INTRODUCTION

1.1.   Background

Rapid developments in the technology of on board satellite sensors need to be accompanied by calibration and validation of the resulting Earth observation data (for instance the upcoming ESA's Sentinel 2 due to be launched in the next 2 years). This is due to the temporal degradation of satellite sensors in-orbit making it difficult to have confidence in pre-flight assigned radiometric values obtained from satellite sensors especially in their usage for the sustainable management of natural resource and climate modelling. For instance, it makes it challenging in dealing with measurements of subtle changes of the Earth. Example: monitoring climate change.

The most effective way of calibrating sensors post-launch is by using standardized calibration sites on the Earth's surface where ground based measurements can be taken and compared with the satellite's observation. A set of principles for using calibration sites has been established by the Committee on Earth Observation Satellites (CEOS) and Working Group on Calibration and Validation (WGCV). Thus, GCTs are required for vicarious calibration (VC) and validation activities. These activities are intended to establish confidence in the quality assurance of remotely sensed products derived from the airborne and spaceborne systems.VC is considered as the means of independently assessing the quality guarantee and accuracy of remotely sensed data products acquired by airborne sensors post-launch (Teillet et al., 1998; Thome, 2004; NCAVEO, 2005; Bannari et al., 2005; Odongo, 2010).

These calibration and validation sites are normally assumed as being large uniform terrain areas located on the Earth. They are also thought of as exhibiting constant reflectance over time, have lambertian reflecting properties and devoid of vegetation. Typical examples of vicarious calibration (VC) sites are ideally dry lake beds or uniform desert areas. The best VC sites are normally located at high altitude which aids in reducing the atmospheric effect (such as aerosols) on the signal (CEOS, 2000;Thome, 2001; Teillet et al., 2001;NCAVEO, 2005).

Several calibration and validation sites are in operation across the globe. Currently, the salt lake site, Tuz Gölü located in Turkey is under investigation as a potential international reference benchmark to evaluate satellites' sensor-to-sensor biases, and also to calibrate and/or validate airborne sensors' radiometric performance (CEOS, 2000; NCAVEO, 2005). The need for a platform to standardize physical measurements acquired by airborne sensors post-launch globally is a fundamental requirement to the ever advancing remote sensing technology which will be

beneficial for environmental modelling and management studies (Bannari et al., 2005; NCAVEO, 2005).

Problems associated with spatial homogeneity and temporal stability of GCTs may lead to a challenge in establishing accurate quantitative calibration and realizing the long-term characterization of the sensor's radiometry (Kneubühler et al., 2006). Furthermore, during sampling of spectral measurements in the field, sources of uncertainty (such as the effect of illumination conditions with time) when characterizing GCTs are rarely investigated. Errors arising from inaccurate calibration do propagate into Earth observation (EO) products used in a wide range environmental modelling and management studies.

As a result of this, decisions related to spatial and multi-temporal analyses, thematic classification and generation of vegetation indices based on these data may be misleading (Bannari et al., 2005). Thus, there is an increasing demand for well-characterised ground targets with respect to their usefulness in vicarious calibration and atmospheric correction processes (Moran et al., 2003; Anderson and Milton, 2006; Kneubühler et al., 2006) and the consequent implications on characterising the quality and accuracy of remotely sensed data products. This calls for a thorough assessment and understanding of the spatial structure dynamics and temporal stability of naturally occurring calibration and validation sites.

1.2.   Problem Statement

It is required that these natural calibration sites should be "spatially homogenous" (Scott et al., 1996;Thome, 2001;Biggar et al., 2003;Bannari et al., 2005;Teillet et al., 2007). However, the terms "spatial homogeneity" needs to be fully defined for a thorough comprehension of the spatial structure of GCTs. Thus, the afore-mentioned property needs to undergo critical scientific investigation to determine its validity – which is crucial with respect to identification and sampling of GCTs. Limited amounts of research have been reported in literature regarding these issues [e.g. (Bannari et al., 2005; Gurol et al., 2008; Odongo, 2010)]. Hence, further developments are required to better the understanding of "spatial homogeneity" of calibration sites and its implications on remotely sensed data products.

1.3.   General objective

This study seeks to identify and investigate "spatial homogeneity" property of GCTs for a thorough understanding of their spatial structure. The study further aims at characterizing the influence of scale (in terms of pixel resolution and window size) measurements on spatial homogeneity property of GCTs by developing and testing methods for its assessment. Thus, the study focuses on characterizing the spatial

domain of GCTs through time across the VNIR and SWIR bands of Landsat TM, MODIS (MOD09A1) and ASTER L1B sensor which is a novelty of this study as an extension of a preliminary study conducted by Odongo (2010).

1.3.1. Research objectives and questions

Research Objectives	Research Questions
1. To investigate the spatial homogeneity property of GCTs.	1. What constitutes spatial homogeneity of ground calibration targets? 2. How should spatial homogeneity of GCTs be measured?
2. To determine how spatial homogeneity varies with wavelength. .	3. How does spatial homogeneity vary across the spectral bands [the visible, infra red and short-wave infrared (SWIR) portions of spectrum] and to what extent is this variation significant? 4. Does the reflectance (HDRF) of GCT surfaces remains invariant across the VNIR and SWIR bands from year to year?
3. To determine how spatial homogeneity varies with scale.	5. How does spatial homogeneity vary with pixel size? 6. How does spatial homogeneity vary with window sizes used to assess spatial structure?

2.   LITERATURE REVIEW

2.1.   Characteristics for selection GCTs

Ground calibration targets (GCTs) are natural earth surfaces or artificial surfaces used for post-launch radiometric calibration of satellite sensors (vicarious calibration) and atmospheric correction (AC). For a surface to qualify as a test site suitable for calibration and atmospheric correction, it has to satisfy the following characteristics (Thome, 2001;Kneubühler et al., 2006;Teillet et al., 2007) :

1. The site should have high spatial uniformity over a large area to minimize mis-registration and adjacency effects due to light scattered from outside the target region.
2. The site should have a reflectance factor (HDRF) greater than 0.3 across all wavelengths averaged over all angles in order to provide higher signal-to-noise ratio (SNR) and reduce uncertainties due to the atmospheric effects.
3. The surface of the site should have flat spectral reflectance to reduce uncertainties due to different spectral response profiles when multiple sensors are involved in cross-calibration.
4. The surface properties of the site (reflectance, BRDF, spectral) should be temporally invariant to reduce BRDF and spectral surface reflectance effects. Otherwise, adequate accuracy would be obtained only if these properties were measured for every calibration.
5. The surface should be horizontal with near-Lambertian reflectance to minimize uncertainties due to different solar illumination and observation geometries. It should also be flat to minimize slope-aspect effects.
6. The site should be located at high altitude (to minimize aerosol loading and the uncertainties due to unknown vertical distribution of aerosols), far from the ocean (to minimize the influence of atmospheric water vapour), and far from urban and industrial areas (to minimize on aerosol loading).
7. The site should be situated in arid regions with low probability of cloudy weather and precipitation that could change the soil moisture and subsequently the surface reflectance. The low probability of cloud coverage also increases the probability of the satellite instruments imaging the test site at the time of overpass.
8. A longer distance to densely populated areas and/or industrial facilities decreases the effect of anthropogenic aerosols.
9. Having a large site minimizes the unwanted effects of scattering of light from areas outside the target area. Instrumented test site that is easily accessible is preferred.

It is difficult for a single test site to have all the aforementioned characteristics. However, of most relevance to the calibration and validation community are points 1, 3 and 4 since characterization of these surfaces are informed on the uncertainties in spectral measurements in the field. Any significant variation in points 1, 3 and 4 will lead to disqualifying such a surface as a candidate test site for VC.

2.2.   Reflectance factor

Field measurements of reflectance can be represented as reflectance factors (Nicodemus et al., 1977). Reflectance measurements have been used to support vicarious calibration [e.g.(Thome, 2001; Six et al., 2004)] atmospheric correction (Moran et al., 2001) and scaling-up measurements to match with satellite derived reflectance (Milton et al., 2009) Reflectance measurements have also been used to develop and validate surface reflectance models (Maignan et al., 2004) and incorporated in process-based modelling and validating biophysical models (Kuusk et al., 2009).
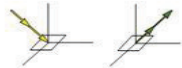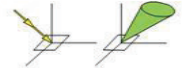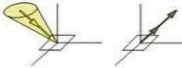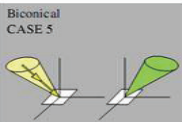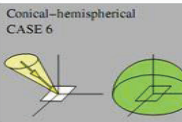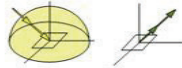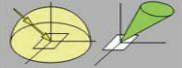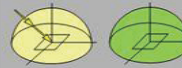
Due to the wide application of reflectance measurements, different reflectance terminologies have been used to inform on spectral measurements in the field by the remote sensing community. This fact, therefore has raised suggestions to the proper use of the terminology (Schaepman-Strub et al., 2006; Milton et al., 2009). Schaepman-strub et al., (2006) argues that to keep in line with advances in spectroscopy, radiometric calibration, atmospheric correction and product development there is need to standardise reflectance terminology and products ascertained. This is in line with the fact that the confusion may lead to uncertainties. Also, not all of the documented reflectance nomenclature (Nicodemus et al., 1977) can be measured in the natural environment and some still remain as concepts (Milton et al., 2009) (See Table 2.1). Nicodemus et al., (1977) further argues that, under natural conditions in the field, single direction incident light measurement is not achievable. This is attributed to diffuse irradiance being highly influenced by the atmosphere and the surface. Thus, directional incidence and reflection will be wrongly estimated as required.

Nonetheless, the argument that a number of reflectance measurements in literature have been documented as bidirectional reflectance function (BRF) and hemispherical directional reflectance factor (HDRF) whereas in essence some reflectance measurements should be termed as hemispherical conical reflectance (HCRF) with respect the mode of measurement (Schaepman-Strub et al., 2006; Milton et al., 2009). Single directional spectral measurements require infinitesimally solid angles of incidence and reflectance. However, all field spectro-radiometers have a finite instantaneous field of view (IFOV) and will always measure HDRF. The approximations of HDRF may be valid if the instrument has a narrow IFOV (3°

or less) and that there are no directional effects within the FOV are explained in literature (Milton et al., 2009). This means that the presumed HDRF measurement will not vary within the FOV for it to qualify as HDRF. Furthermore, the target surface should be homogenous. In view of this, it is reasonable that documentation be made describing; (i) the IFOV of instrumentation used in spectral measurements and (ii) homogeneity of target surfaces measured. This would help to support the correct inference and usage of reflectance products.

Nicodemus, (1977) and Schaepman-Strub et al., (2006) noted that proper documentation is useful in ensuring the proper standardization of reflectance terminologies. This also creates awareness of the uncertainties associated with the different reflectance products. For example, climate models have been found sensitive to specification of surface albedo, with accuracies ranging from ±0.02 to ±0.05, regarded as suitable (Oleson et al., 2003). In this regard, standardization of the reflectance quantities and products will be useful in ensuring that the right choice of reflectance products are integrated in modelling approaches and that users will be aware of uncertainties existing where there is need to fuse or compare different reflectance products from different sensors (e.g. MODIS BRDF/albedo product MOD43B, MISR reflectance products). This study is based on HDRF associated with satellite measurements.

Table 2.1: *Relation of incoming and reflected radiance terminology used to describe reflectance quantities*

Relation of incoming and reflected radiance terminology used to describe reflectance quantities. The labelling with 'Case' corresponds to the nomenclature of Nicodemus et al. (1977). Grey fields correspond to measurable quantities (Cases 5, 6, 8 and 9); the others (Cases 1–3, 4 and 7) denote conceptual quantities Source: Schaepman-Strub et al., (2006).

2.3.   Uncertainty in measurement of reflectance factor

Uncertainty in the scientific field can be broadly classified into two categories, namely (i) uncertainty in understanding (i.e. knowledge based) processes functionality and (ii) uncertainty in measurements which is normally ascertained by ascribing either the degree of error or the degree of accuracy to values obtained from measurements (Foody, 2001; Foody and Atkinson, 2002; Zhang and Goodchild, 2002).   Uncertainty in measurement can also be   defined as "A parameter associated with the result of a measurement that characterizes the dispersion of the values that could reasonably be attributed to the measurand (i.e. quantity)" (Fox, 2001; Fox, 2009). Thus, the focus of this study is a characteristic of uncertainty in measurement with much emphasis on variation. Some uncertainties may arise from infeasibility of characterizing some atmospheric correction parameters (e.g. aerosol content) due to financial constraint.

Evaluation of variation (herein referred to as uncertainty) in measurements of reflectance is necessary because of its usefulness in ensuring confidence in the measured value. Uncertainty should characterize the range of values within which the true value is speculated to lie. This can be realized by accounting for all possible effects; both random and systematic (Fox, 2009). There is the need to accompany delivered EO products with documentation of uncertainty stating their confidence levels and traceability to a reference standard. In the case of reflectance measurements in the field, the white Spectralon™ panel is normally used to anchor traceability of measurements to national and/or international standards (CEOS, 2010) in order to account for errors that may arise in the reflectance measurements.

Quantitative studies of uncertainty associated with reflectance measurements of surfaces in the field has been the foundation of evaluating the quality of EO products acquired simultaneously from space-borne and airborne sensors. Distinctions in uncertainty respecting variation in measurement can categorized as (a) those arising from inherent surface response (i.e. roughness or smoothness) and (b) those from apparent illumination and viewing conditions (i..e. degree of clarity in the sky) (Anderson and Milton, 2005; Anderson, 2005). The inherent properties here refer to uncertainty due to the structure of the surface and their spectral-dependent properties (Gao et al., 2003) whereas apparent illumination and viewing conditions are attributed to the changes in the distribution of hemispherical irradiance (Kriebel, 1976).

The causes of uncertainty due to inherent surface response include surface moisture variations, growth of plant and other biological material on the surface, weathering and erosion of the surface (Anderson and Milton, 2006). Bannari et al., (2005) and Kneubuhler et al., (2006) acknowledged that, these factors have been known to

influence the optical properties, homogeneity and stability of ground calibration test site.

2.4. Spatial homogeneity and temporal stability properties of GCTs

Ground calibration targets (GCTs) are of prime importance to the calibration and validation of Earth observation data measurements acquired by airborne and spaceborne systems. The GCTs are never selected by chance but have to meet a set of defined characteristic requirements established by the Committee on Earth Observation Satellites Working Group on Calibration and Validation (CEOS WGCV) (CEOS, 2000; Kneubühler et al., 2006; Gurol et al., 2008; Pegrum, 2008).

Among these characteristic requirements are the spatial homogeneity and temporal stability of GCTs. These properties of GCTs are crucial to the long term characterization of satellite sensor radiometry and subsequent implication on decision making processes based on derived remotely sensed data products (Scott et al., 1996; Rondeaux et al., 1998; Thome et al., 1998). Thus, an evaluation of the aforementioned properties is an important requirement during the usage of GCTs for sensor calibration (Thome, 2001;De Vries et al., 2007;Teillet et al., 2007).

Spatial homogeneity is viewed broadly as the state or characteristic of a surface to be made up of the same constituents (i.e. the condition of all things/entities in a group being of the same kind). Spatial homogeneity simply refers to identified areas/surfaces with similar reflectance values within an image (Bannari et al., 2005). Thus, the spatial homogeneity of GCTs denotes uniformity over extended area of several pixels in all directions (Rondeaux et al., 1998). Its relevance is envisaged in cross-calibration between sensors due its role in reducing mis-registration, and adjacency effects of the different sensors (Teillet et al., 2007).

Kneubuhler et al., (2006) argues that temporal stability of GCTs characterizes a surface to exhibit constant reflectance over time. This implies that such a surface should depict invariability (unchanging) in measured spectra over time. Inter and intra annual (temporal) stability of referenced sites is vital for vicarious calibration and sensor inter-calibration process. Thus, the absence of temporal stability (i.e. presence of large temporal variability) in a surface would lead to a situation where spectral measurements need to be collected always during a calibration process in order to attain adequate calibration results (Scott et al., 1996; Teillet et al., 2007).

Spatial homogeneity and temporal stability of GCTs may be considerably affected by factors such as surface moisture variations, presence of vegetation or lichens which result in spectral changes, variation terrain structure (topography) introducing shady effects and surface dryness which causes cracks. These factors may introduce

variation when characterizing reference sites (Slater et al., 1987; Biggar et al., 1994; Thome et al., 1998; Kneubühler et al., 2006).

Uncertainties associated with spatial and temporal variability of surfaces are known to greatly affect aerosol optical thickness retrieval employed in atmospheric correction processes (Guoyong et al., 1999). Furthermore, Guoyong et al., (1999) envisaged that an increase in spatial homogeneity size of a surface corresponds to a reduction in the uncertainty level of mean aerosol optical thickness as adjacency effects become insignificant. Guoyong et al., (1999) findings indicated that given an aerosol optical thickness of less than 2 and a surface reflectance of less than 0.12, uncertainty level in the aerosol optical thickness is about 5-20 times, the errors in surface reflectance.

2.5.   Spatial homogeneity and temporal stability assessment

Spatial homogeneity structure of a GCT can be characterized using global and local indicators/measures of spatial autocorrelation and also the coefficient of correlation method. Global spatial statistics produce an overall pattern between proximity and the similarity of pixel values. These statistics provide a measure of the spatial autocorrelation of the dataset as a whole in a global manner (Bannari et al., 2005; Spiker and Warmer, 2007). This is useful in characterizing the spatial structure of surfaces. The three commonly used global spatial statistics comprise of Moral's I, Geary's C and Semi-variance.

- The Moran's I index compares the differences between neighbouring pixels and the mean to provide a measure of homogeneity. The value range is between +1 and -1, where +1 = strong positive spatial autocorrelation (homogeneity), 0 = spatially uncorrelated data, and -1 = strong negative spatial autocorrelation.
- The Geary's C index compares the differences between neighbouring pixels to the standard deviation to provide a measure of dissimilarity within a dataset. The value range is between 0 and 2. Where 0 = strong positive spatial autocorrelation, 1 = spatially uncorrelated data, and 2 = strong negative spatial autocorrelation.
- The semi-variance is simply half the expected squared variance of the differences between all possible points spaced at a constant distance apart and thus expresses the degree of relationship between points on a surface (Woodcock et al., 1988; Spiker and Warmer, 2007).

A correlogram or variogram is useful is studying/establishing how observed pattern of spatial autocorrelation decrease with increasing distance (Curran, 1988). These plots consist of autocorrelation statistics calculated at various lag distances

displayed against the lag. When using the Moran's I or Geary's C statistics, this plot is called a correlogram; when using the semi-variance statistics, this plot is called a variogram. In this study, the semi-variance and Geary's C index statistics were used to explore the spatial structure of Tuz Gölü. These global measures of spatial autocorrelation potentially ignore important local variation within a given dataset and thus gives a single value which is representative of the overall spatial interrelations of the area under investigation (Wulder and Boots, 1998; Bannari et al., 2005; Spiker and Warmer, 2007).

 In view of this, Getis and Ord (1992) introduced a local autocorrelation measures: *Gi* and *Gi** statistics. *Gi* statistic excludes the reflectance value (HDRF) of the pixel (i.e. pixel "*i*") under consideration at a particular point in time from the local sum computation whilst the *Gi** takes into account the HDRF of such a pixel. Anselin (1995) subsequently proposed *local indicators of spatial autocorrelation* (LISA) useful for decomposing global autocorrelation measurements so that the individual contribution of each observation (sample unit) can be computed within the entire imagery. These methods also make it possible to assess local "clusters/patches" or areas of spatial homogeneity (similarity) and heterogeneity (dissimilarity) within an image (Wulder and Boots, 1998; Bannari et al., 2005).

The coefficient of variation (CV) is a widely used statistic in determining temporal variability of GCTs (De Vries et al., 2007). In imagery, CV is calculated within a predefined local window (e.g. 3×3 window size) by moving the window over the entire image under investigation. The use of CV in characterizing the radiometric temporal stability of GCTs (examples: La Crau site in France, Railroad Valley Playa site in United States, Newell County Rangeland in Canada and Lunar Lake playa in United States) are documented by Gu et al., (1992), Telliet et al.,(1998) and Bannari et al., (2005).

A surface with a CV of 3% or less is considered to be temporally stable and thus temporally stable within the computed window (Cosnefroy et al., 1996; Bannari et al., 2005; Kneubühler et al., 2006). However, CV computation can be misleading in determining a spatially uniform and temporally stable surface. This situation arises when two or more connected surfaces may be considered to have same CV value implying that they are spatially uniform, but may not exhibit homogeneity. Hence, other spatial indices which could adequately characterize spatial uniformity and temporal stability should be explored to enhance characterization of GCTs. Thus, a combination CV and Getis Ord statistic was used to characterize the spatial homogeneity structure of Tuz Gölü.

3. STUDY SITE AND DATA PREPARATION

3.1. Rationale (Why Tuz Gölü?)

Tuz Gölü (Lake Tuz) site located in southern Turkey exhibits characteristics of any other lake for ten months of the year. However, during July and August, the lake dries to become a bright, pristine, white surface, which is ideal for calibrating Earth observation satellites. There is vegetation near the lake but there is no vegetation inside the lake that can deteriorate spectral and temporal uniformity. The drying up of the lake during summer minimize the influence of atmospheric water vapour (Gurol et al., 2008; Pegrum, 2008).

Tuz Gölü is large horizontal site which minimizes the unwanted effects of scattering of light from areas outside the target area. The site is easily accessible. The site is already instrumented with a weather station, GPS and Spectroradiometer. Thus, Tuz Gölü is listed among the eight test sites recently endorsed by the Committee on Earth Observation Satellites (CEOS) to become an international reference standard to evaluate satellites' sensor-to-sensor biases, and also to calibrate/validate their radiometric performance(National Physical Laboratory, 2010).

3.2. Description of GCT employed in the study: Tuz Gölü Lake

Tuz Gölü Lake (Figure 3.1) is a potential vicarious calibration site in Turkey, Europe. This GCT is an ephemeral saline lake. The lake is the second biggest lake in Turkey, covering a peak area of 1,500 km^2 for most periods throughout the year area with very shallow depth in appearance. Its area coverage is approximately 80 km long and 50 km wide. The lake is located on geographical coordinates of 38 50^{0}N and 33 20^{0}E which correspond to the central Anatolian region, approximately 105 km north east of Konya and 150 km south east of Turkish capital Ankara. Its altitude is approximately 905 m above mean sea level. The prevailing sunny and cloud- free atmospheric conditions during summer months of July – August characterize the site's suitability for VC and atmospheric correction activities (Gurol et al., 2008; Mustafa and Soğanci, 2010). Currently (referring to August, 2010), there are on-going campaigns by the calibration community geared towards characterization of Tuz Gölü site for VC and atmospheric correction purposes.
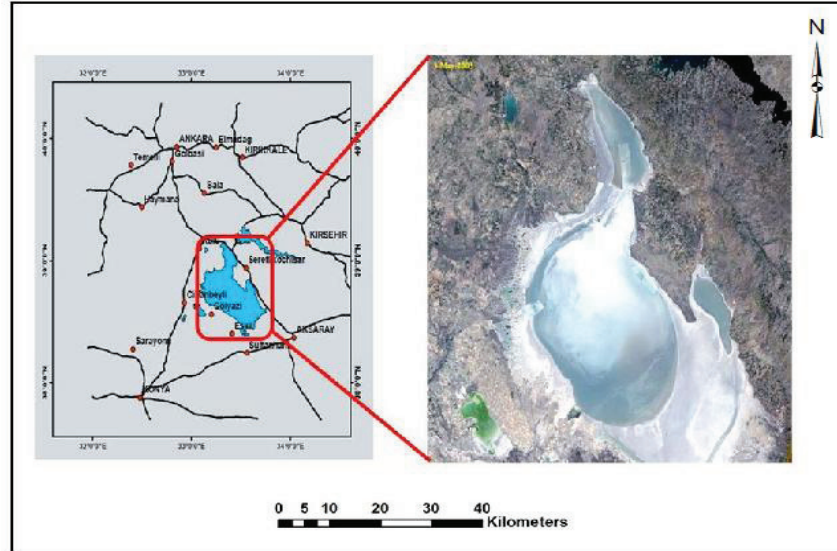
Figure 3.1: Location map and its Landsat ETM (Bands 1 – 7) composite map of Tuz Gölü Lake, Turkey. Source: Adapted from USGS website, 2009. Source: http://calval.cr.usgs.gov/images/sites_catalog/tuzg/tuzGolu.pdf

3.3. Satellite data acquisition and image processing

Landsat TM, MODIS TERRA (MODO901A) and ASTER (ASTER L1B Registered Radiance at the Sensor data product) satellites' images of Tuz Gölü test site were acquired from the Land Processes Distributed Active Archive Centre (LPDAAC) and the Warehouse Inventory Search Tool (WIST) of National Aeronautics and Space Administration (NASA) websites. These websites are under the auspices of the United States Geological Survey (USGS).

Time series images of the aforementioned satellites were chosen in order to derive spectral reflectance values specifically the Hemispherical Directional Reflectance Factors (HDRF) within the Visible and Near Infrared (VNIR) and the Shortwave Infrared (SWIR) portions of the Electromagnetic Spectrum for spatial homogeneity and temporal stability assessment of Tuz Gölü calibration site. The following considerations were fundamental in the selection of the satellite images. They include:

- Priority was given to datasets captured within the months of July and August due to the fact that, the test site normally dries up within these

months making it useful for vicarious calibration purposes. However, ASTER images of the months of April and October were also collected due to lack of availability of enough ASTER scenes for the months of July and August.

- The percentage of cloud cover of the captured scenes/images was of prime concern. Thus, images of least cloud cover percentage were selected. The chosen images fall within cloud cover percentages of 0 – 9.
- The pixel resolutions of the selected images were based on the satellite sensor's resolution being fine and coarse. The Landsat TM images were at 30 meters resolution for its VNIR, SWIR and Thermal Infrared (TIR) bands. The MODIS TERRA (MODO901A) had a resolution of 500 m for all its VNIR and SWIR eight bands. The ASTER images comprised of 15 m resolution for its four VNIR bands, 30 m resolution for its six SWIR bands and 90 m resolution for its five TIR bands.

3.4. Satellite datasets preparation

The prime focus of the study aims at investigating the spatial homogeneity structure of Tuz Gölü test across the VNIR and SWIR bands of the aforementioned three different satellite sensors. Thus, it was necessary to eliminate the TIR bands. Layer stacking and resizing (pixel aggregation) of the wavelength bands was carried out in ENVI^{TM} Version 4.7 software.

For the Landsat datasets, the sensor's bands 1, 2, 3, 4, 5 and 7 (Table 4.1) corresponding to the VNIR and SWIR bands were resized and the layers (bands) stacked together into one single image comprising of six bands leaving out band 6 which is the TIR band (Figure 4.1).

The ASTER datasets comprised of 15 bands: the first four bands represent VNIR bands, the 5th band to the 10th band representing the SWIR bands and the remaining five bands constitute the TIR bands. A single image comprising of 14 bands (see: Appendix 2) was produced through resizing and layer stacking leaving out one of the VNIR. The eliminated band is a near infrared backward- scanning band (Figure 4.1). It is normally tagged as Band 3B. This band is useful in creation of a stereo view of the earth for elevation studies and should be avoided during spatial statistical analysis or classification purposes (CEOS, 2010; The Yale Center for Earth Observation, 2010).

The MODIS datasets (MOD09A1: Surface Reflectance 8-Day Level 3 Global 480m) is a derived product of the MODIS Surface- Reflectance Product (MOD09). The dataset is computed from the MODIS Level 1B having spectral bands of 1, 2, 3, 4, 6 and 7 which centred at 648 nm, 858 nm, 470 nm, 555 nm, 1240 nm, 1640

nm, and 2130 nm respectively (see: Table 3.1). The product constitutes an estimate of the surface spectral reflectance for each band as it would have been recorded at ground level under conditions of no atmospheric scattering or absorption. The product is a processed data where radiometric and atmospheric correction and Bi-directional Reflectance Function (BDRF) have been corrected. The dataset is at a resolution of 480 m and has Sinusoidal map projection. The correction scheme provides amendments for the effect of atmospheric gases, aerosols, and thin cirrus clouds; it is applied to all non-cloudy MOD 35 Level 1B pixels that have passed the Level 1B quality control (MODIS Data Product Handbook, 2009).

The correction procedure is based on using band 26 to detect cirrus cloud, water vapour from MOD 05, aerosol from MOD04, and ozone from MOD07. Thus, in the absence of the MODIS water vapour, aerosol and/or ozone products, the best-available climatology is embarked on. Also, the correction also employs the MOD43, BRDF without topography, captured the previous 16-day time period for the atmosphere-BRDF coupling effects (MODIS Data Product Handbook, 2009). An eleven year MOD09A1 datasets comprising the year 200 - 2010 for the months of July and August were acquired. These datasets coordinate system were transformed from Sinusoidal projection to WGS-84 having the Universal Transverse Mercator (UTM) Zone 36N projection.

The projected datasets and atmospheric corrected datasets were then resized by pixel replication procedure (using the "Resize Data" option in ENVI and "Pixel aggregate" options) from fine resolution to coarse resolution. The reason for considering the different spatial resolutions (30 m, 240 m, 480 m and 1000 m) was to find out whether the site can be useful for the calibration of a wide range of sensors resolutions (i.e. for both fine and coarse resolutions).

Table 3.1: *Description of the spectral range of bands and spatial resolution for MODIS TERRA (MODO901A: Surface Reflectance 8-Day Level 3 Global 480 m).*

MODIS	Wavelength (μm)	Resolution(m)
Band 1 (Red)	0.63 - 0.69	480
Band 2 (NIR)	0.78 - 0.90	480
Band 3 (Blue)	0.45 - 0.52	480
Band 4 (Green)	0.53 - 0.61	480
Band 5 (NIR)	1.23 - 1.25	480
Band 6 (SWIR)	1.55 – 1.75	480
Band 7 (SWIR)	2.09 - 2.35	480

Source: http://activefiremaps.fs.fed.us/region4/modis_bands.html

3.5.   Atmospheric and Radiometric Correction

Atmospheric and Topographic Correction software (ATCOR-2) was employed in the radiometric and atmospheric correction of the selected Landsat TM and ASTER images (Table 3.2 - 3.4). In order to establish a standardized platform with respect to the obtained surface reflectance values of Tuz Gölü test site during the radiometric and atmospheric correction procedure, standard estimates and parameters of the atmospheric profiles were entered in ATCOR-2 (Appendix 1). The spectral signatures of vegetation, bare ground and water features found in each atmospherically corrected image were analyzed and compared to their standardized reflectance patterns (i.e. the spectral signatures of vegetation, bare ground and water features) in the VNIR and SWIR portions of the spectrum (Figure 3.2). These procedures were useful in minimizing errors in the obtained surface reflectance values due to lack of field spectral measurements.

3.5.1.   Landsat TM and ASTER images

The flat terrain algorithm of ATCOR-2 was used for the radiometric and atmospheric correction of the Landsat and ASTER datasets. A total of 21 Landsat images and 8 ASTER scenes of different years were used in the operation (see table 3. 2 - 3.4).

Table 3.2: *Description of the spectral range of bands and spatial resolution for the TM sensor*

Landsat TM	Wavelength (µm)	Resolution(m)
Band 1 (Blue)	0.45 - 0.52	30
Band 2 (Green)	0.52 - 0.60	30
Band 3 (Red)	0.63 - 0.69	30
Band 4 (NIR)	0.76 - 0.90	30
Band 5 (SWIR)	1.55 - 1.75	30
Band 6 (TIR)	10.40 – 12.50	120
Band 7 (SWIR)	2.08 - 2.35	30

Source: Adapted from http://eros.usgs.gov/#/Guides/landsat_tm

The images were in the band sequential (BSQ) format. The geographical coordinate system of the datasets was geo-referenced to WGS-84 datum and Universal Transverse Mercator (UTM) Zone 36N projection. The atmospheric correction procedure employed here was based on a typical atmospheric correction workflow outlined by Richter (2007). The resulting 30 m×30 m pixel resolution ASTER datasets (after atmospheric and radiometric correction using ATCOR-2) were then

resized by pixel replication procedure from a pixel resolution of 30 m × 30 m to 240 m × 240 m, 480 m × 480 m and 1000 m ×1000 m.

The atmospheric corrected ASTER images had a total of 10 bands comprising of 3 VNIR bands, 6 SWIR bands and 1 TIR band (see: Appendix 2). The TIR band corresponds to ASTER TIR band13 which is normally characterized with no data because it acts as an input file for ATCOR with respect to the spectral emissivity correction. The emissivity is normally set to a constant value of 0.98 for the surface brightness temperature computation (Richter, 2007). The resulting 15 m × 15 m pixel resolution ASTER datasets (after atmospheric and radiometric correction using ATCOR-2) were then resized by pixel replication procedure from a pixel resolution of 15 m × 15 m to 30 m × 30 m.

Table 3.3: *Time series Landsat TM data obtained from LPDAAC for August*

Date (YY-MM-DD)	Time (GMT)	Cloud (%)	Sun Elevation Angle (SEA) in degrees
1984-08-03	7:50: 51	0	56.61
1984-08-26	7:57: 40	0	51.80
1985-08-13	07:57:19	0	54.75
1987-08-19	7:53:48	0	53.12
1989-08-16	8:01:06	0	54.72
1998-08-01	8:05:59	0	58.46
1998-08-17	8:06:07	0	55.34
2003-08-15	8:04:35	0	55.57
2003-08-31	8:04:54	0	51.84
2007-08-10	8:21:03	0	59.07
2009-08-15	8:16:57	0	57.27
2010-08-18	8:17:58	0	57.27

Table 3.4: *Time series ASTER Level 1B data obtained from LPDAAC website*

Date (YY-MM-DD)	Time (GMT)	Cloud (%)	SEA (degrees)
2001-04-27	8:55: 12	4	62.66
2004-04-12	8:38: 46	1	56.41
2004-04-12	8:38:54	1	56.94
2004-08-02	8:38:33	4	63.05
2005-07-27	8:44:28	0	65.32
2005-10-08	8:37:58	6	43.19
2005-10-08	8:37:07	9	43.78
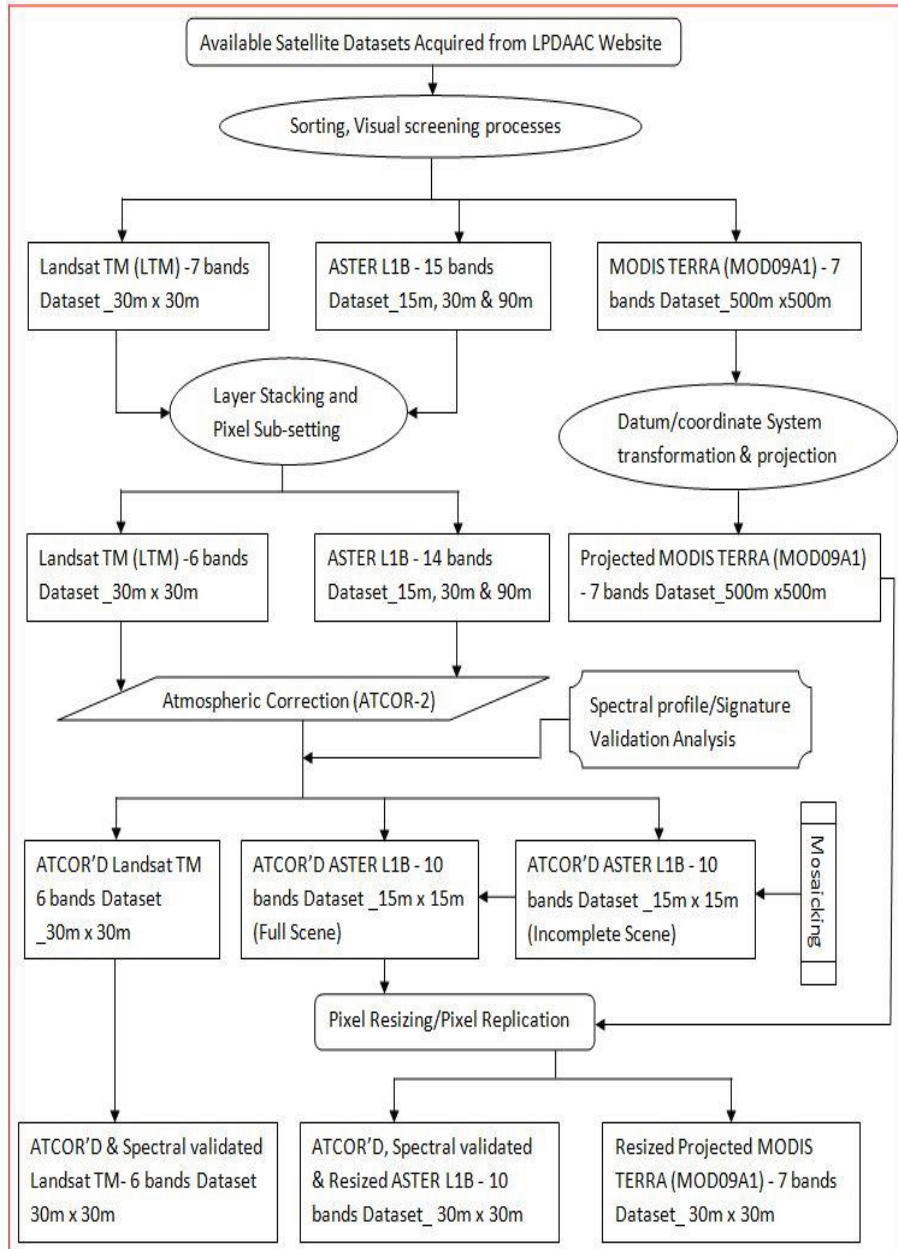
Figure 3.2: Satellite Image Acquisition and Pre-Processing of Landsat TM, ASTER L1B and MODIS datasets of Tuz Gölü.

4.   METHODOLOGY

4.1.   Characterizing the spatial structure of Tuz Gölü

In this study, variograms and Geary C index statistic were used to explore the spatial structure of Tuz Gölü using the Landsat TM and MODIS images. ESRI ArcGIS™ version 10 and ENVI™ version 4.7 were used to compute the variograms and correlogram for the VNIR and SWIR bands of Landsat TM and MODIS.

In ENVI, the lag distance was specified in pixels during the correlogram computation. The Geary's C autocorrelation statistic was then calculated at each lag distance, up to the specified maximum lag. For example, a value of 4 means that autocorrelation will be calculated for lags of 4, 3, 2, 1 and for each pixel's nearest neighbours. In all the Geary's C statistical computation, the Queen's neighbourhood criterion was used. The Queen's criterion was preferred because it defines the neighbourhood as comprising all eight adjacent pixels in the directions of the rows, columns, and diagonals respectively. This gives a measure of the pattern averaged over all directions (Spiker and Warmer, 2007).

Also, trend analysis was conducted to explore and determine whether there exist patterns in the reflectance (HDRF) measurements across Tuz Gölü respecting the Landsat TM VNIR and SWIR bands. This was carried out by building transects from north to south, west to east, northwest to southeast and southwest to northeast directions (Figure 4.1) across Tuz Gölü using Landsat TM image captured in August, 2010 as an input file in ENVI^{TM} Version 4.7. Scatterplots were then generated respecting each direction by plotting the reflectance (HDRF) or pixel value (y-axis) against the point location of the pixel (x-axis). The direction of increment/decrement in the reflectance distribution across the lake is crucial to building sampling techniques geared towards the selection of suitable fields/areas within TG for vicarious calibration activities.

4.2.   Spatial homogeneity assessment

Gi* statistic returns positive values for pixels surrounded by clusters of relatively high reflectance while negative values are surrounded by clusters of relatively low reflectance. This ability to highlight brighter pixels within a given image makes the Gi* advantageous and particularly useful in characterizing ground calibration targets. Thus, Gi* combines spatial association and relative spectral response from imagery in comparison to other local indicators of spatial autocorrelation (LISA) such as Geary's *c* and Moran's *I*. These brighter pixels are fundamental to vicarious calibration and atmospheric correction activities which depend exclusively on the

use of relatively high reflectance values that are brighter than average (Wulder and Boots, 1998; Bannari et al., 2005; Spiker and Warmer, 2007; Gurol et al., 2008).

The Gi* values are calculated by using the formula below within a local distance predefined using four different kernels (i.e. small, medium and large pixel window sizes) by employing an IDL™ routine code in RTW tools created by Wilson (2009).

$$Gi^*(d) = \frac{\sum w_{ij}(d)x_j - Wi^*\bar{X}}{s[Wi^*(n-Wi^*)/(n-1)]^{\frac{1}{2}}}$$

Where:

n represents the number of the observations (pixels) within the image.

$w_{ij}(d)$ is a matrix of spectral weights with binary and symmetric having a weight equal to unity ($w_i = 1$) for all pixels found within distance d of pixel i considered and a weight equal to zero ($w_{ij} = 0$) for all pixels found outside d. $\sum w_{ij}(d)x_j$ is the sum of varying values x (i.e. reflectance of the imagery) within distance d of pixel i. Wi^* is the number of pixels within the distance d with pixel i included.

s is the variance of x, and $\bar{x}$ is the global mean of x.

The Gi* distance d are determined at 3×3, 5×5, 7×7 and 9×9 pixel windows respectively. The different window sizes indicate the area confinement (i.e. the extent of the area with the entire image) where Gi* is computed. A small window size (3×3) depicts that the spatial dependency among the dataset is confined to localized regions. A large window on the other hand depicts that the spatial dependency is viewed within a wide region (Bannari et al., 2005). In this study, the small window (3×3) will be used for the spatial homogeneity assessment of Tuz Gölü. This will be useful in identifying localized clusters of homogeneous areas with pixel values/ reflectance (HDRF) that are relatively brighter than average. Gi* will be calculated for the VNIR and SWIR bands in each imagery (Figure 4.2).

Gi* value range greater than zero (average reflectance value) representing positive reflectance values (Brighter pixels) were then extracted by overlaying all the Gi* output maps for the VNIR and SWIR bands respectively for all the years. This was important since it ensured the extraction of areas within Tuz Gölü that have remained spatially homogeneous throughout the years. Spatial Analyst™ in ESRI ArcGIS™ was used for this analysis. The output was a single map showing the areas of spatial homogeneous with respect to the VNIR and SWIR bands.

4.3. Temporal stability assessment

The Coefficient of Variation (CV) will be used to investigate how reflectance in homogeneous areas identified varies over yearly time-scale.

Variation in the HDRF will be assessed using formula below:

$$cv = \frac{s}{\bar{x}}$$

Where:

s is the standard deviation of the HDRF and $\bar{x}$ is the mean of the HDRF.

Variation in HDRF was determined in different kernels of 3×3, 5×5, 7×7 and 9×9 pixel using IDL™ routine code in RTW tools created by Wilson (2009). CV was calculated for the VNIR and SWIR bands for all the available satellite images (Landsat TM, MODIS and ASTER). It has been established that areas that are temporally stable within a given imagery will have a coefficient of variation of less than 3% (Gu et al., 1992;Teillet et al., 1990;Bannari et al., 2005). Therefore, in this study, homogeneity will be assigned to areas within Tuz Gölü having CV values of less than 3% (Figure 4.2).

Patches/areas matching less than 3% local variation within the 3x3 window were extracted for the VNIR and SWIR bands using ESRI spatial analyst™ and overlaid on the spatially homogeneous (Gi* > 0) areas. Areas with CV values less than 3% that coincide with the spatially homogeneous areas were then categorised as being temporally stable with minimal subtle variations in HDRF across the 3x3 window.

Eventually, a large extent of the area was found as being homogeneous and stable over time and space. This area was oriented coincidently with the satellite path to avoid any mis-alignment of pixels within the area. This area can considered as the most suitable area within Tuz Gölü for vicarious calibration and atmospheric correction activities.

4.4. Choice of window size for spatial homogeneity assessment

The different window sizes indicate the area confinement (i.e. the extent of the area within the entire image) where the Getis Ord statistic is computed. A small window size (3×3) depicts that the spatial dependency among the dataset is confined to a much localized regions. A large window on the other hand depicts that the spatial dependency is viewed within a wide region (Bannari et al., 2005).

In this study, the small window (3×3 is preferred for the spatial homogeneity assessment of Tuz Gölü. This will be useful in identifying patches of homogeneous areas (with pixel values/ reflectance (HDRF) that are relatively brighter than average) within the entire than large windows size (5×5, 7×7 and 9×9) where the pixel viewed within a wide region. These brighter pixels are fundamental to vicarious calibration and atmospheric correction activities (Wulder and Boots, 1998;Bannari et al., 2005;Gurol et al., 2008).
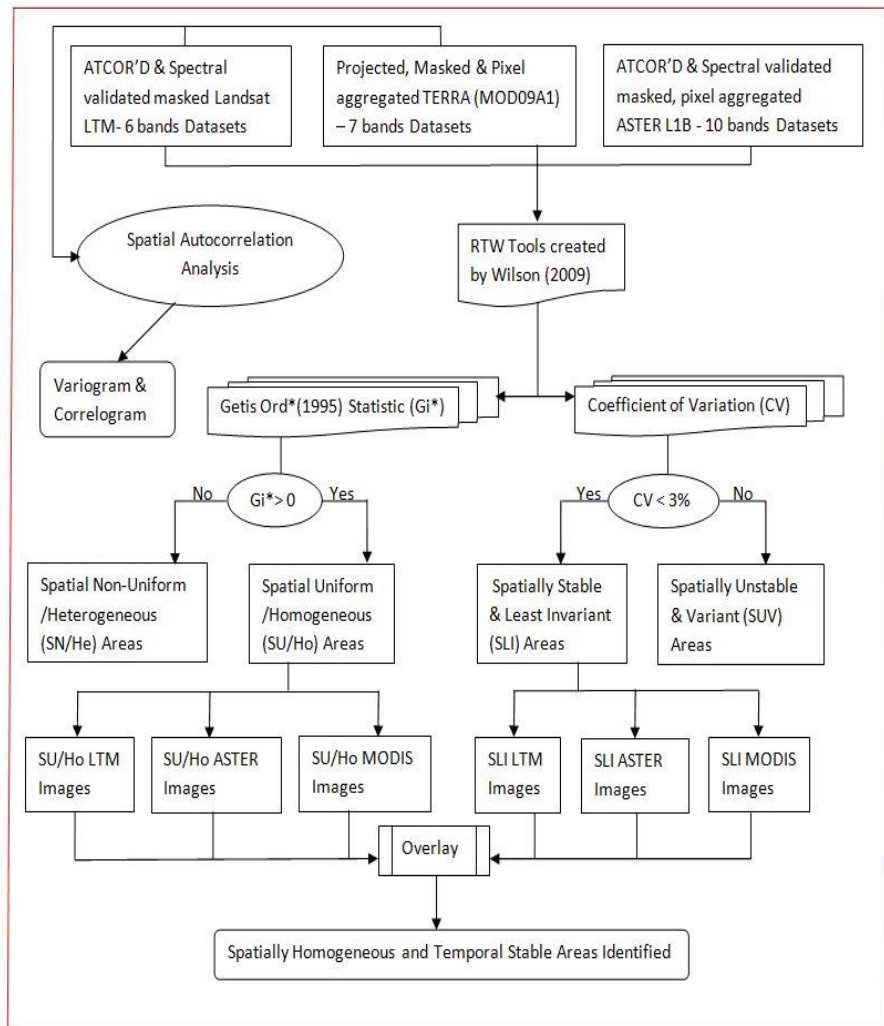
Figure 4.1: Characterization of spatial homogeneity and temporal structure of GCTs for sampling reflectance for vicarious calibration.

5.   RESULTS

5.1.   Trend in HDRF measurements observed across Tuz Gölü respecting Landsat TM bands
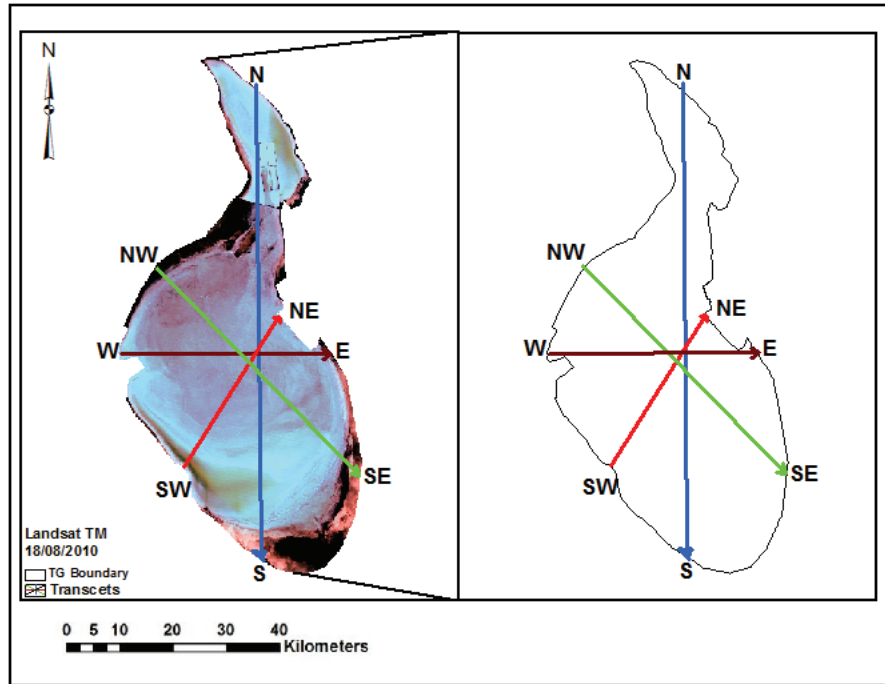
Figure 5.1: Transects created across Tuz Gölü Lake using Landsat TM image of August, 2010 at 30 m resolution. The image is displayed as a true colour composite.

Four transects were created across TG to explore the trend of reflectance (HDRF) respecting the Landsat TM VNIR and SWIR bands (Figure 5.1). The longest transect was from north to south which is approximately 60 km. The west to east transect had a length of 30 km. The northwest to southeast and southwest to northeast transects had lengths of approximately 42 km and 24 km respectively. The purpose of creating the transects is closely linked to understanding the spatial structure of GCTs which is geared towards answering research questions 1 and 2 mentioned in section 1.3.1. It was observed that the VNIR bands had higher reflectance value range (150 – 255) whilst the SWIR bands had lower reflectance value range (20 – 100) across all directions.
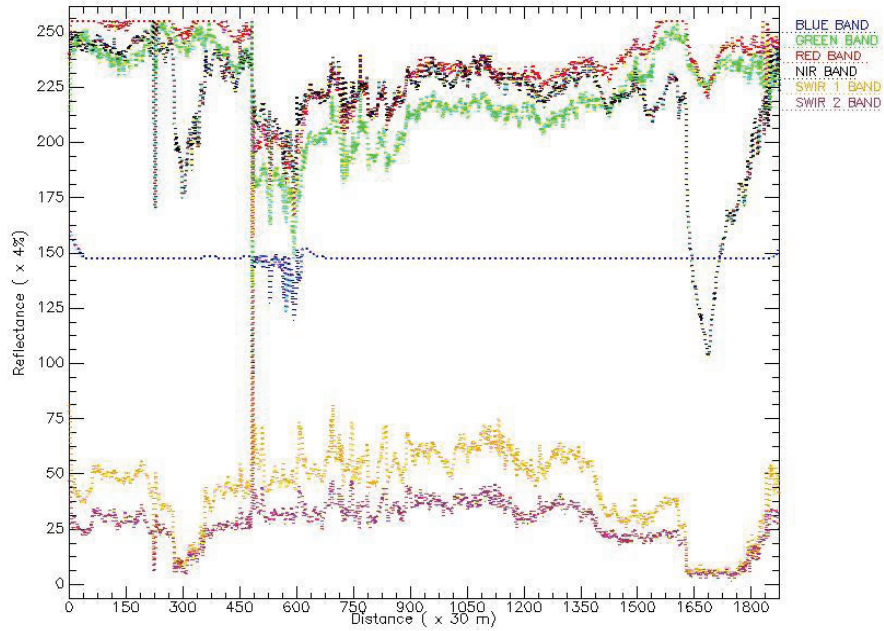
Figure 5.2: Scatterplot of transect across Tuz Gölü from north to south showing pattern observed in reflectance of Landsat TM bands at 30 m resolution.
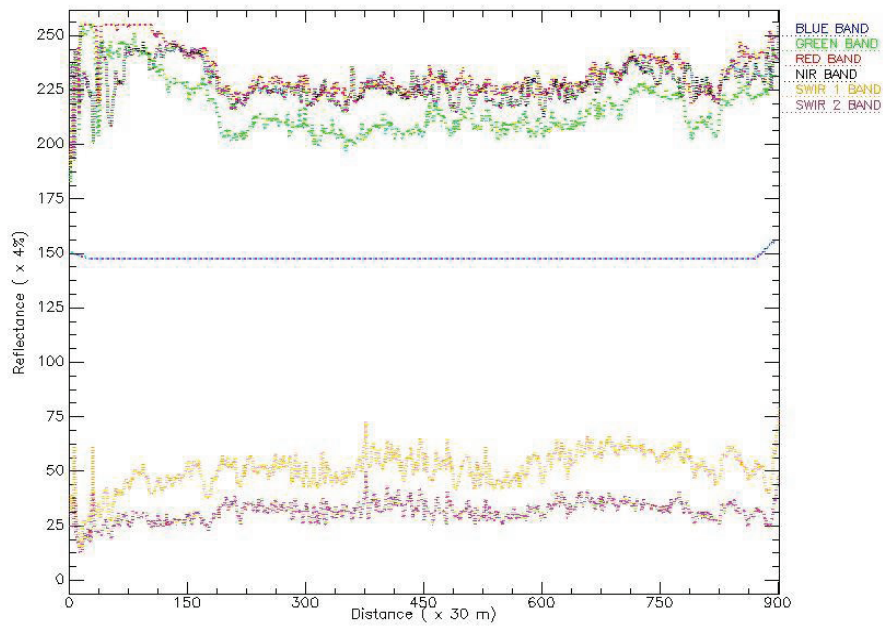
Figure 5.3: Scatterplot of transect across Tuz Gölü from west to east showing pattern observed in reflectance of Landsat TM bands at 30 m resolution.
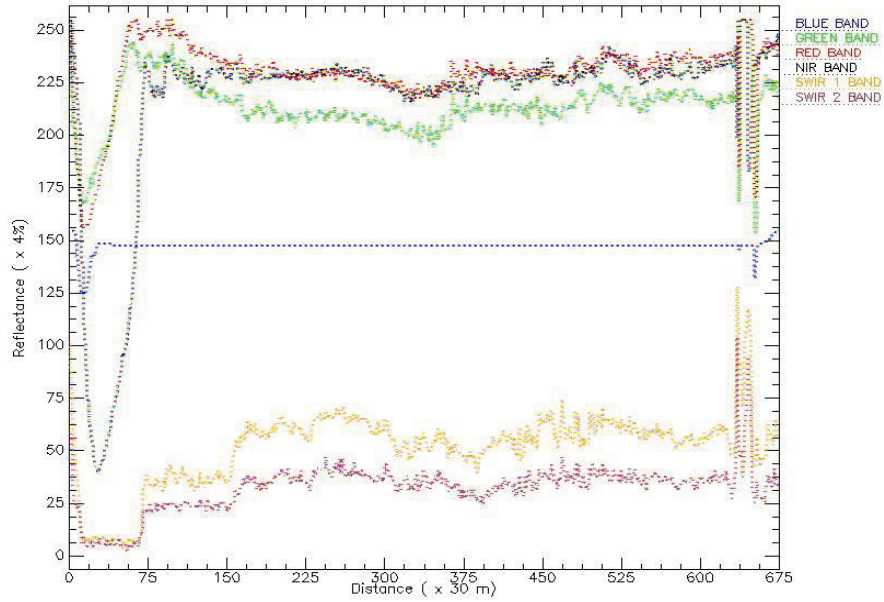
Figure 5.4: Scatterplot of transect across Tuz Gölü from southwest to northeast showing pattern observed in reflectance of Landsat TM bands at 30 m resolution.
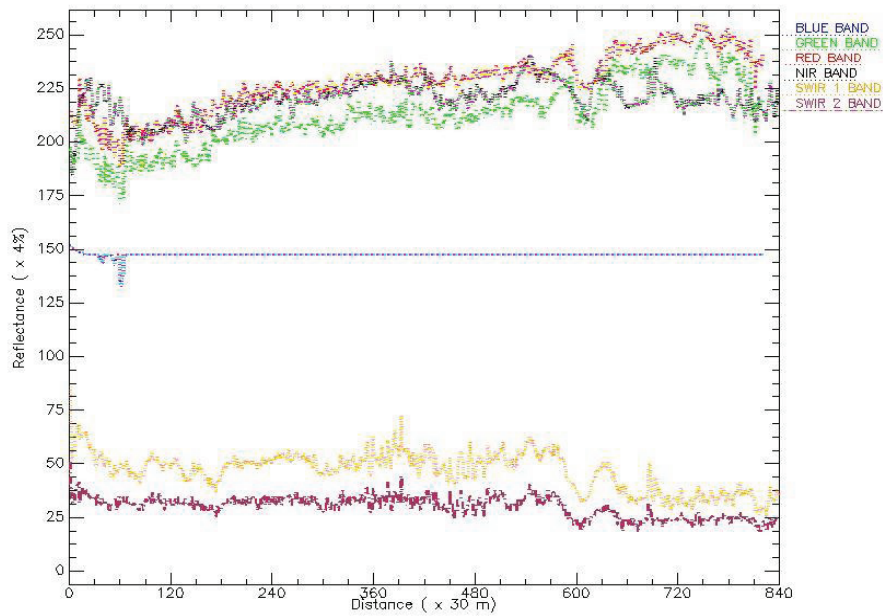
Figure 5.5: Scatterplot of transect across Tuz Gölü from northwest to southeast showing pattern observed in reflectance of Landsat TM bands at 30 m resolution.

5.2. Variograms of Landsat TM bands imagery of Tuz Gölü

The computed variogram of the bands depicts short and long ranges of gradual increment in variation of the HDRF measurements with increasing lag distance. However, two patterns were observed. The short range structure increment in variation is envisaged over approximately 10 km, whilst the long range structure begins from approximately a distance of 20 km and ends at approximately 35 km. Secondly, a stepwise increment in variation until a lag distance of 35 km is reached (Figure 5.6). A similar pattern was observed for the VNIR and SWIR bands for all the Landsat TM datasets captured in July and August. The variograms were computed to explore the spatial autocorrelation structure of recorded HDRF measurement across Tuz Gölü. The creation of the variogram and correlogram were to explore the spatial autocorrelation structure of Tuz Gölü. This is closely linked to understanding the spatial structure of GCTs which is geared towards answering research questions 1 and 2 mentioned in section 1.3.1.
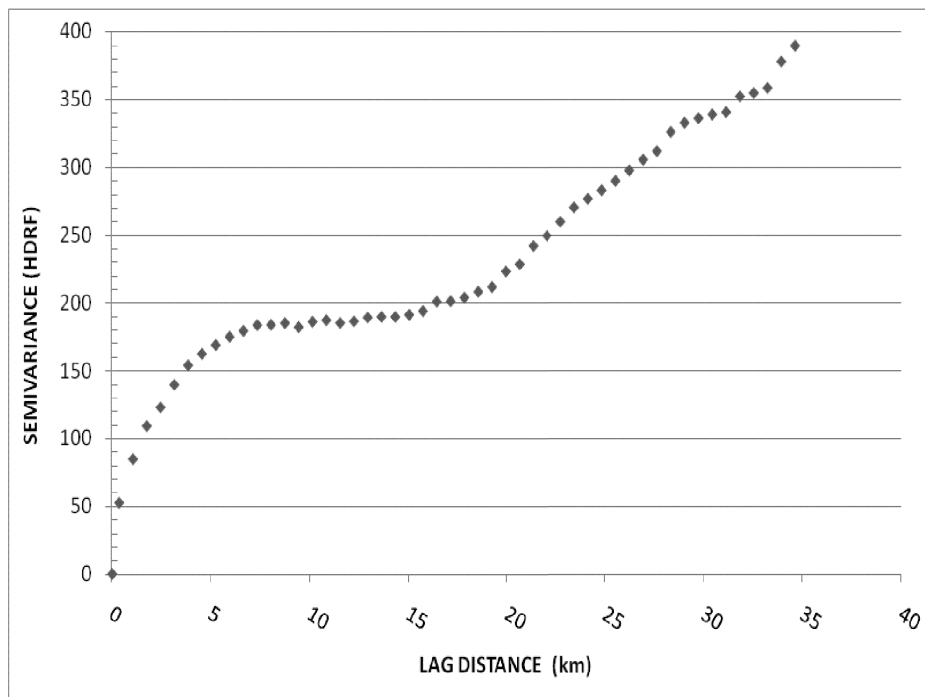
Figure 5.6: Sample variogram of Landsat TM band 1 HDRF variation across Tuz Gölü Lake at 30 m pixel resolution. The image was captured on 18th August, 2010.
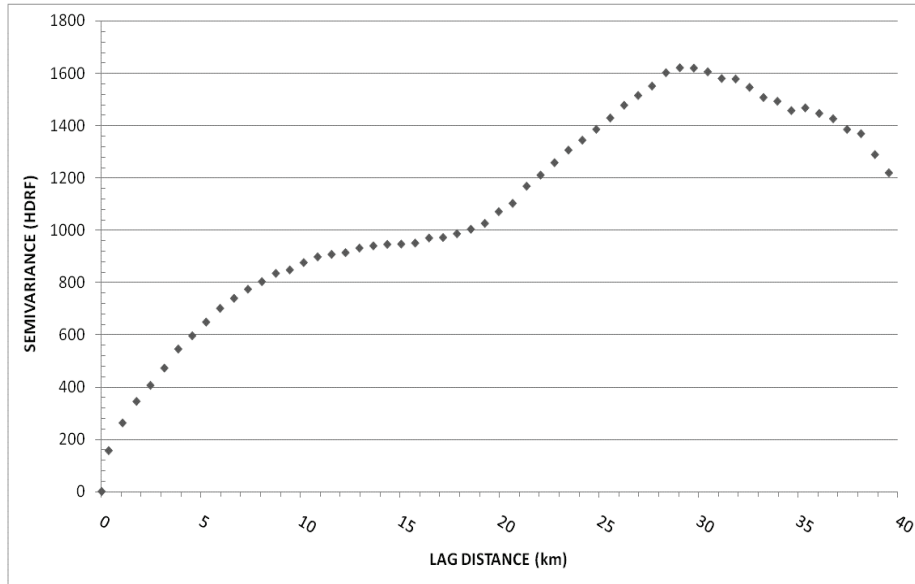
Figure 5.7: A variogram of Landsat TM band 2 HDRF variation across Tuz Gölü Lake.
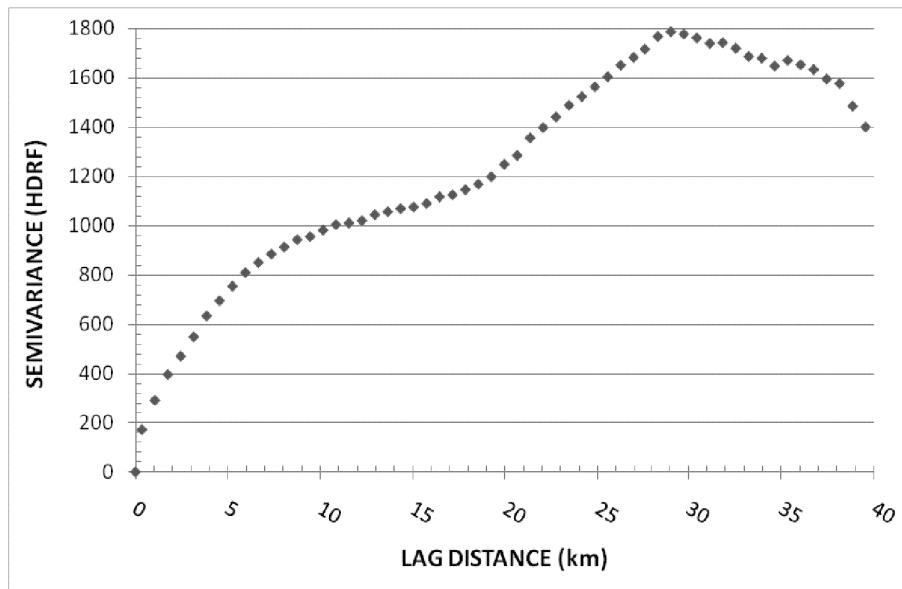
Figure 5.8: A variogram of Landsat TM band 3 HDRF variations across Tuz Gölü Lake
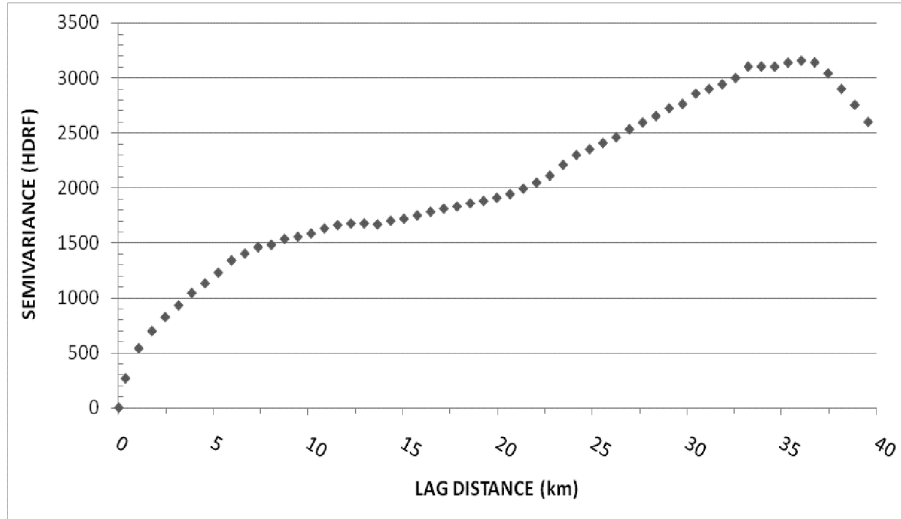
Figure 5.9: A variogram of Landsat TM band 4 HDRF variation across Tuz Gölü Lake
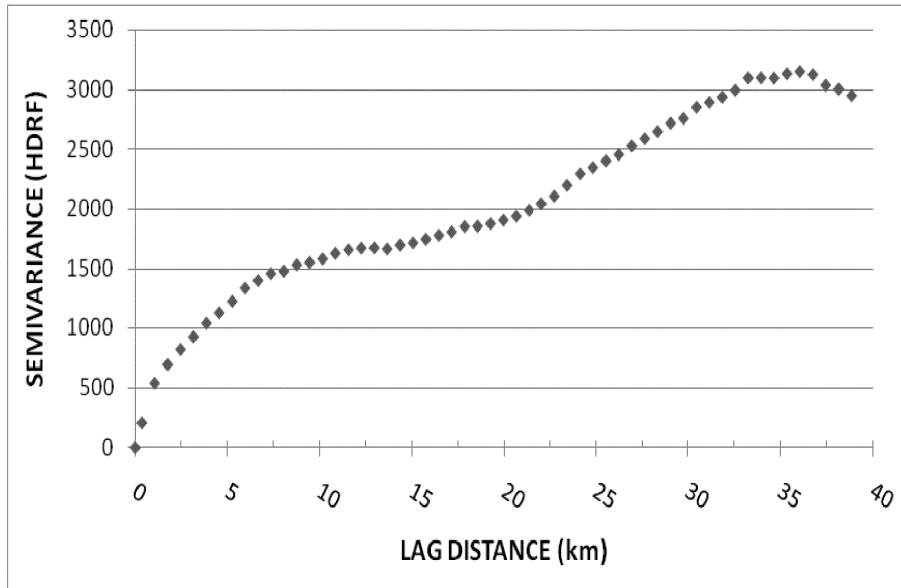
Figure 5.10: A variogram of Landsat TM band 5 HDRF variation across Tuz Gölü Lake
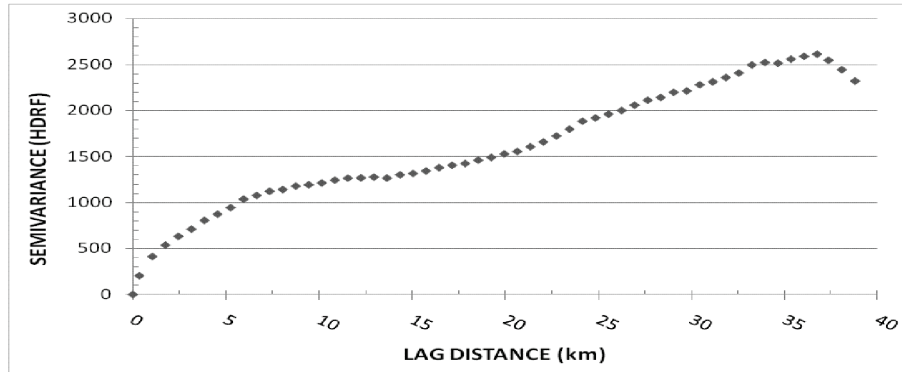
Figure 5.11: A variogram of Landsat TM band 7 HDRF variation across Tuz Gölü Lake

5.3. Correlogram of Landsat TM bands at different resolutions

5.3.1. Geary's C autocorrelation analysis

The Geary's C autocorrelation values increases with increasing lag distance from 0.05 to 0.85 with respect to the VNIR and SWIR bands of Landsat TM .The computed Geary's C values for the visible bands (1, 2 and 3), the infrared band (4) and SWIR bands (5 and 7) ranges from approximately 0.05 to 0.6, 0.1 to 0.7 and 0.1 to 0.85 respectively (Figure 5.12). The computed correlogram was used to explore the spatial autocorrelation structure of recorded HDRF measurement of the VNIR and SWIR bands across Tuz Gölü. The correlogram covers a maximum lag distance of 7.5 km [i.e. the total pixels (250) multiplied by the resolution (30 m)].
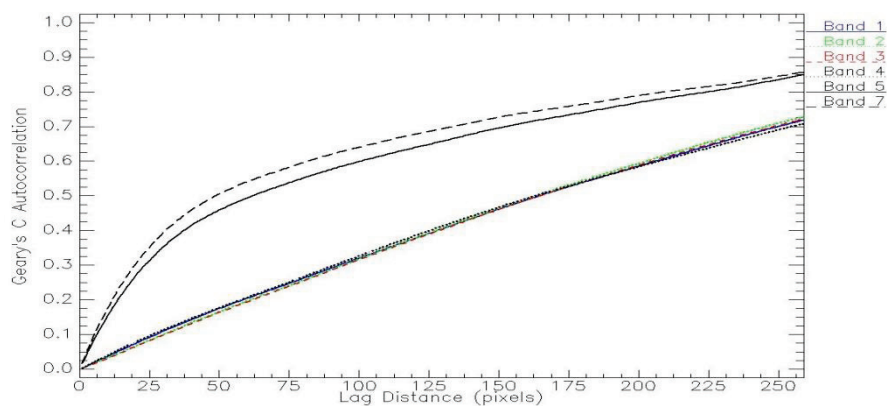
Figure 5.12: Geary's C correlogram of 18/08/2010 Landsat TM VNIR and SWIR bands HDRF variation across Tuz Gölü Lake at 30 m pixel resolution.

5.3.2. Comparing the spatial autocorrelation patterns of VNIR and SWIR bands of Landsat TM and MODIS at 480m pixel resolution using Geary's C indexing method

The Visible and Near Infrared (VNIR) together with the Shortwave Infrared (SWIR) bands of Landsat TM image acquired on 18/08/2010 whose pixel resolution has being aggregated to 480 m were compared with MODIS Terra Surface Reflectance (MOD09A1) image (acquired on 13/08/2010) at the same resolution. The results shows that, the VNIR bands of both sensors exhibit a similar spatial autocorrelation patterns having Geary's C index values ranging from 0.05 – 0.75 (Figure 5.13 - 5.16). In contrast, the SWIR bands of the sensors display variation in their spatial autocorrelation patterns (Figure 5.17 and 5.18).
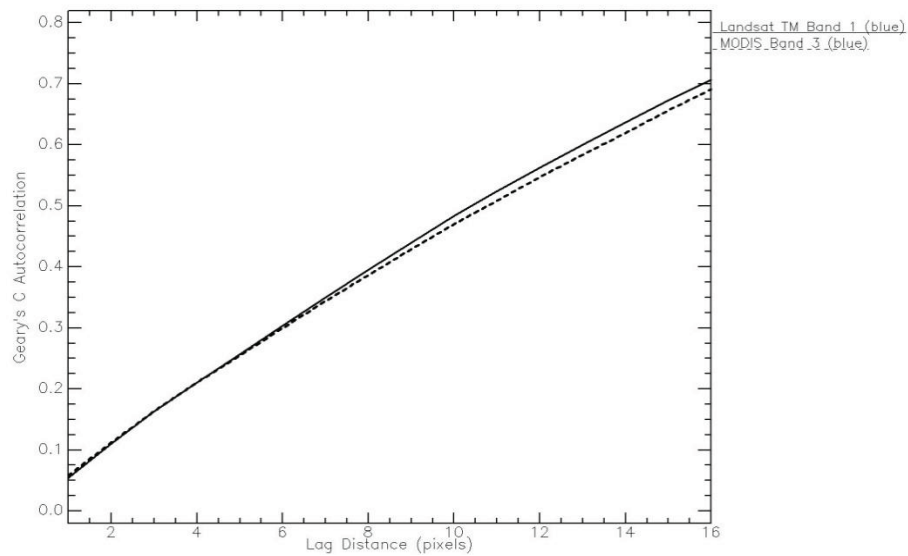
Figure 5.13: Geary's C correlogram of Landsat TM and MODIS blue band HDRF variation across Tuz Gölü Lake at 480m pixel resolution. The Landsat TM and MODIS images were captured on 18/08/2010 and 13/08/2010 respectively.
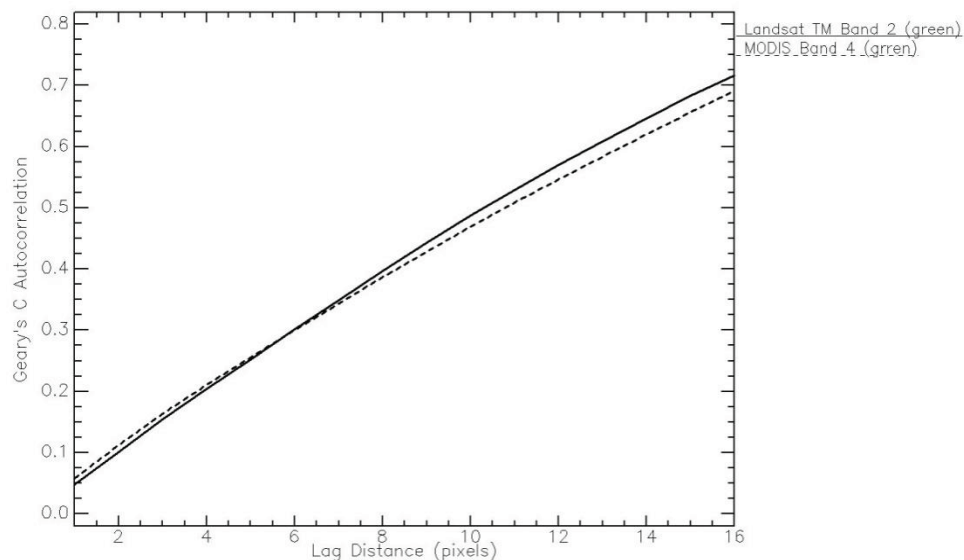
Figure 5.14: Geary's C correlogram of Landsat TM and MODIS green band HDRF variation across Tuz Gölü Lake at 480m pixel resolution. The Landsat TM and MODIS images were captured on 18/08/2010 and 13/08/2010 respectively.
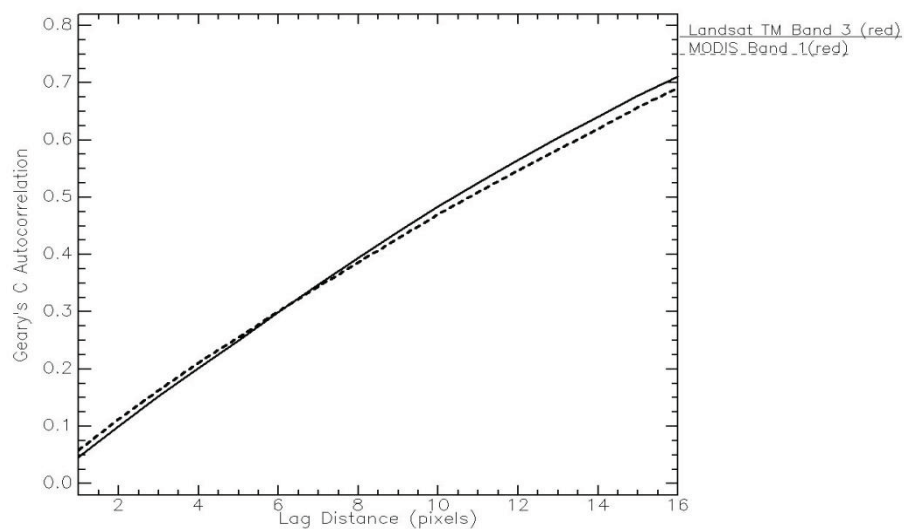
Figure 5.15: Geary's C correlogram of Landsat TM and MODIS red band HDRF variation across Tuz Gölü Lake at 480m pixel resolution. The Landsat TM and MODIS images were captured on 18/08/2010 and 13/08/2010 respectively.
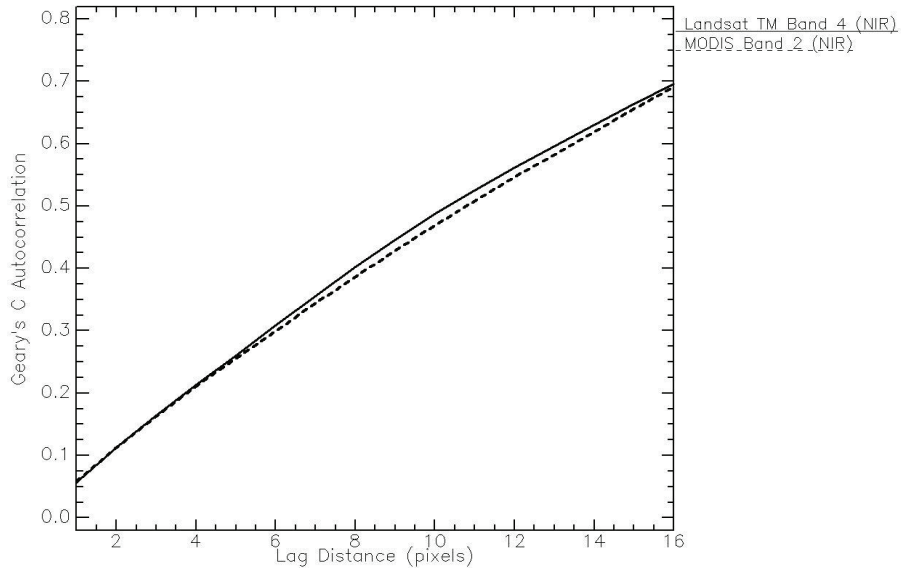
Figure 5.16: Geary's C correlogram of Landsat TM and MODIS NIR band HDRF variation across Tuz Gölü Lake at 480m pixel resolution. The Landsat TM and MODIS images were captured on 18/08/2010 and 13/08/2010 respectively.
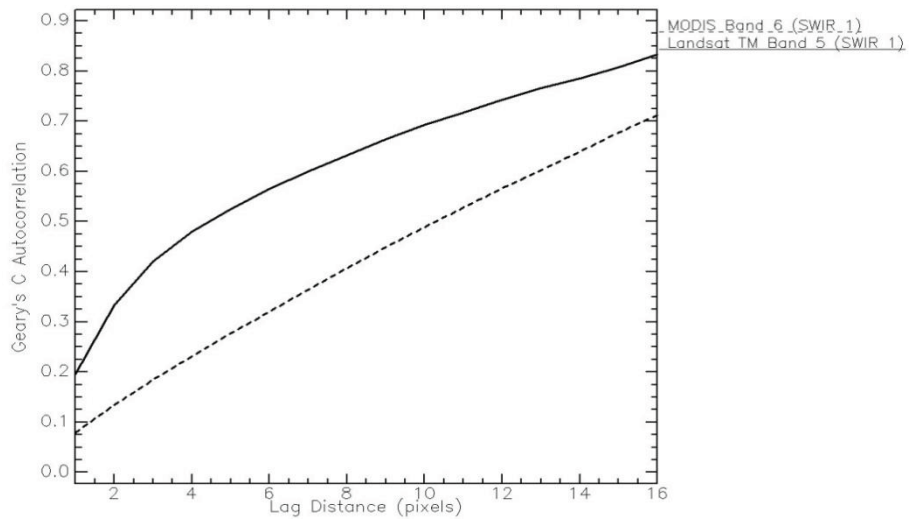
Figure 5.17: Geary's C correlogram of Landsat TM and MODIS SWIR band HDRF variation across Tuz Gölü Lake at 480m pixel resolution. The Landsat TM and MODIS images were captured on 18/08/2010 and 13/08/2010 respectively.
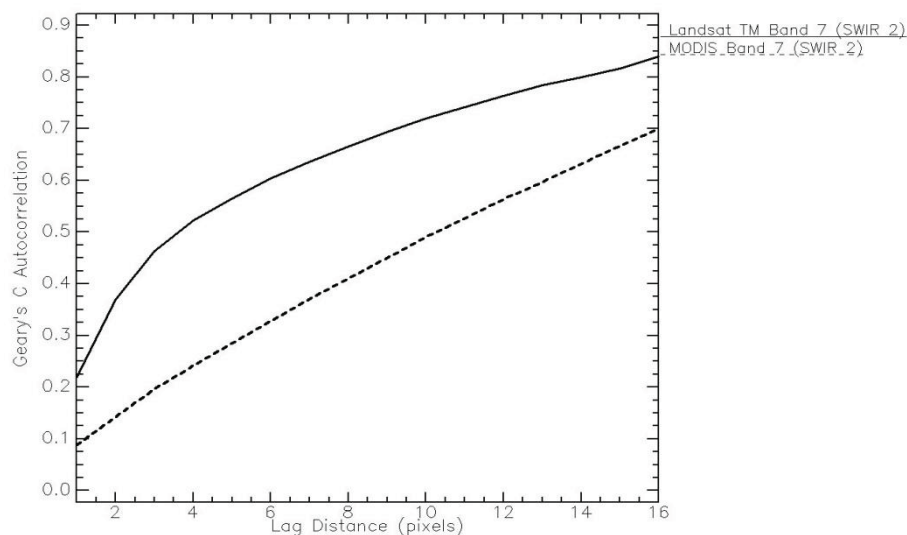
Figure 5.18: Geary's C correlogram of Landsat TM and MODIS SWIR band 7 HDRF variation across Tuz Gölü Lake at 480m pixel resolution. The Landsat TM and MODIS images were captured on 18/08/2010 and 13/08/2010 respectively.

5.4. Spatial homogeneity and temporal stability analysis

5.4.1. Coefficient of variation (CV) and Getis Ord (Gi*) indexes across Tuz Gölü

CV and Gi* computations were carried out on the processed satellite datasets (Landsat TM, ASTER and MODIS images) that has been masked to the extent of Tuz Gölü within a 3×3 localized window. CV value range of 0 to 3 across all the VNIR and SWIR bands was obtained for the 3 aforementioned satellites throughout the months of July and August for all the years with available data (see: Appendix 3, 4, 5, 6, 7, 11and 12). The observed CV range from 0 to 300% across the Landsat TM bands shows that there is a lot variation across the lake surface. Thus, a further extraction analysis with which CV was set to less than 3% (i.e. CV < 3%) in ArcGIS^{TM} using the "raster calculator" was carried out on all the images. This gave patches of areas (Figure 5.19, 5.20, 5.22) within Tuz Gölü that are temporally stable useful for vicarious calibration (Bannari et al., 2005; Kneubühler et al., 2006; Teillet et al., 2007). The extracted areas obtained for the VNIR and SWIR bands were then overlaid through time in order to identify areas that were consistently stable over time across the VNIR and SWIR bands (Figure 5.20 and 5.22, Appendix 8 and 9).

One the other hand, a surface is considered to be spatially homogeneous having a high reflectance value /brighter pixels when it has value of Gi* > 0 as recommended by Bannari (2005). The extracted areas having Gi*> 0 respecting Landsat TM VNIR and SWIR bands (Figure 5.21, and 5.22) were then overlaid through time in order to identify areas that has being spatially homogeneous over time across the VNIR and SWIR bands (Figure 5.23 and 5.24). The results of the SHC analysis were useful in characterizing the spatial homogeneity of Tuz Gölü across the VNIR and SWIR bands. This is closely linked to understanding the spatial structure of GCTs which was geared towards answering research questions 3 and 4 mentioned in section 1.3.1.
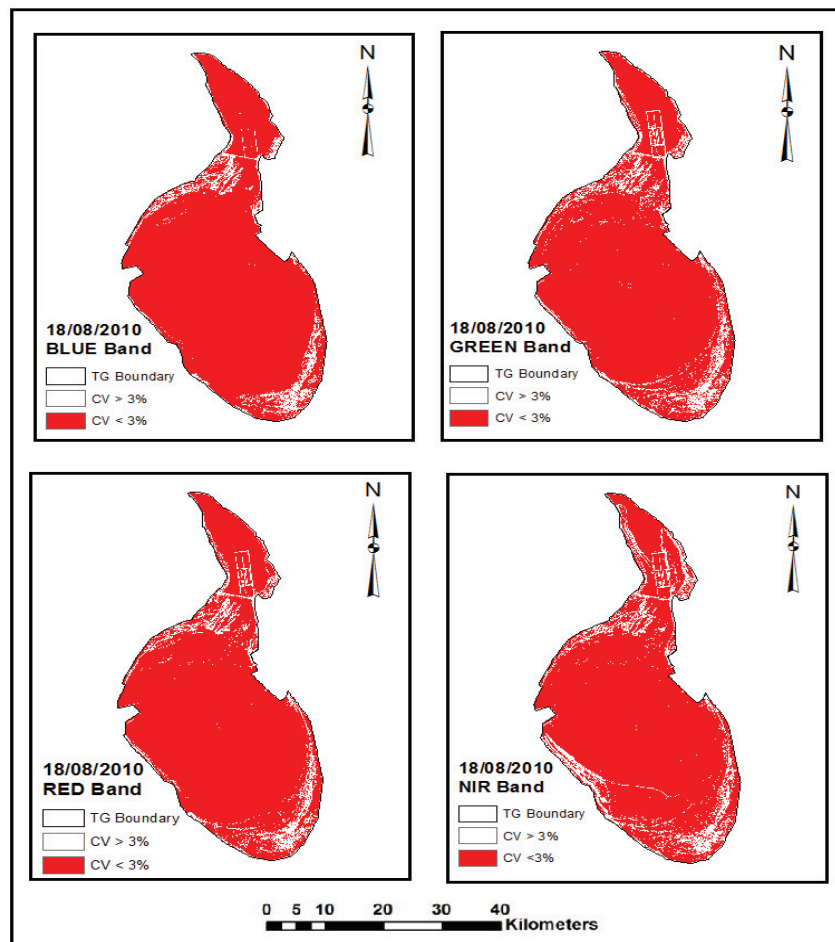
Figure 5.19: CV (%) index map of Tuz Gölü showing Landsat TM VNIR bands at 30 m pixel resolution for the month of August 2010.
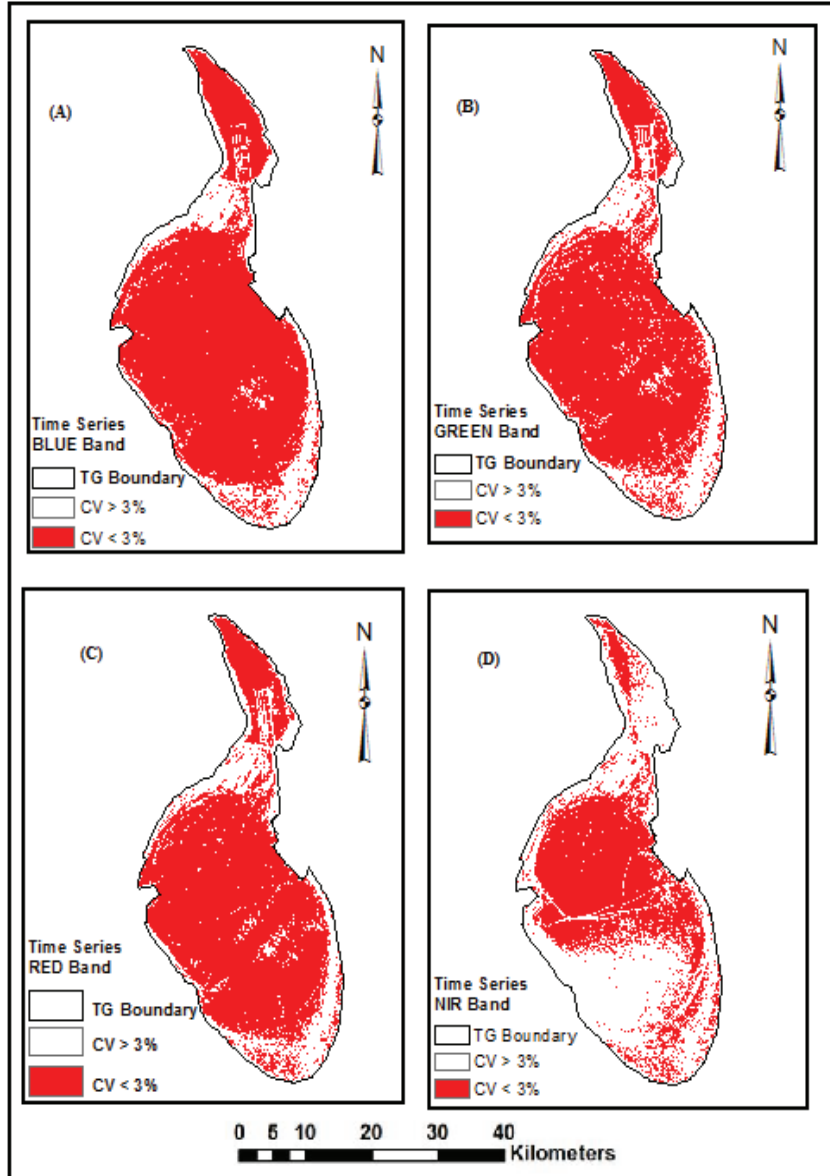
Figure 5.20: Time series CV < 3% map of Tuz Gölü based on Landsat TM VNIR bands for the month of August composed of years 1984, 1985, 1987, 1989,1998, 2003, 2007, 2009 and 2010.
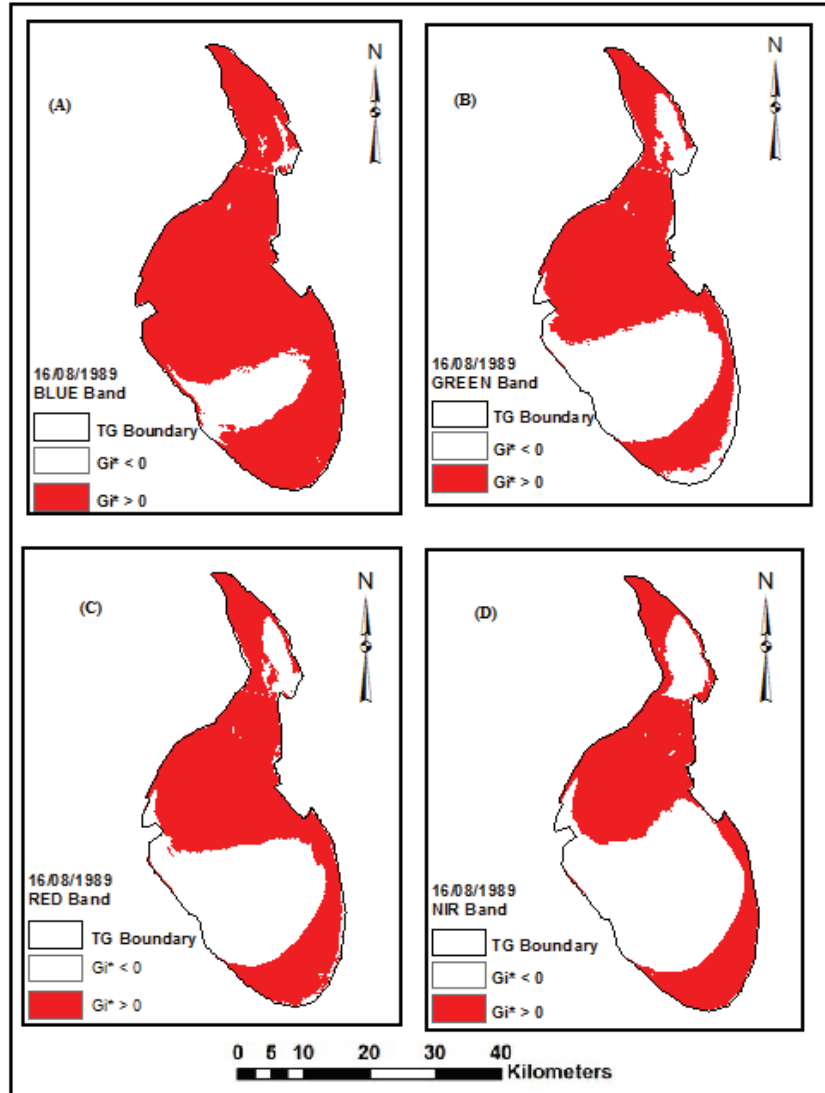
Figure 5.21: Gi* > 0 map of Tuz Gölü showing Landsat TM VNIR bands at 30 m pixel resolution for the month of August 1989.
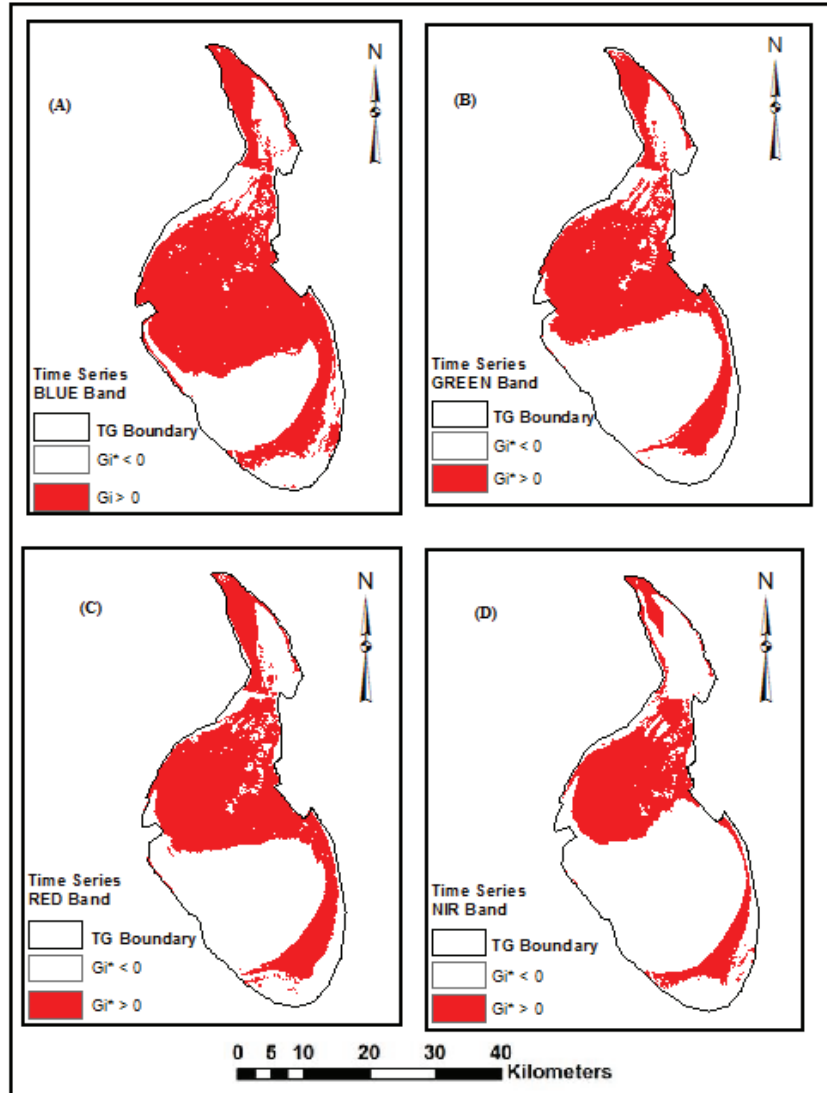
Figure 5.22: Time series Gi* > 0 map of Tuz Gölü based on Landsat TM VNIR bands for the month of August composed of years 1984, 1985, 1987, 1989, 1998 2003, 2007, 2009 and 2010.
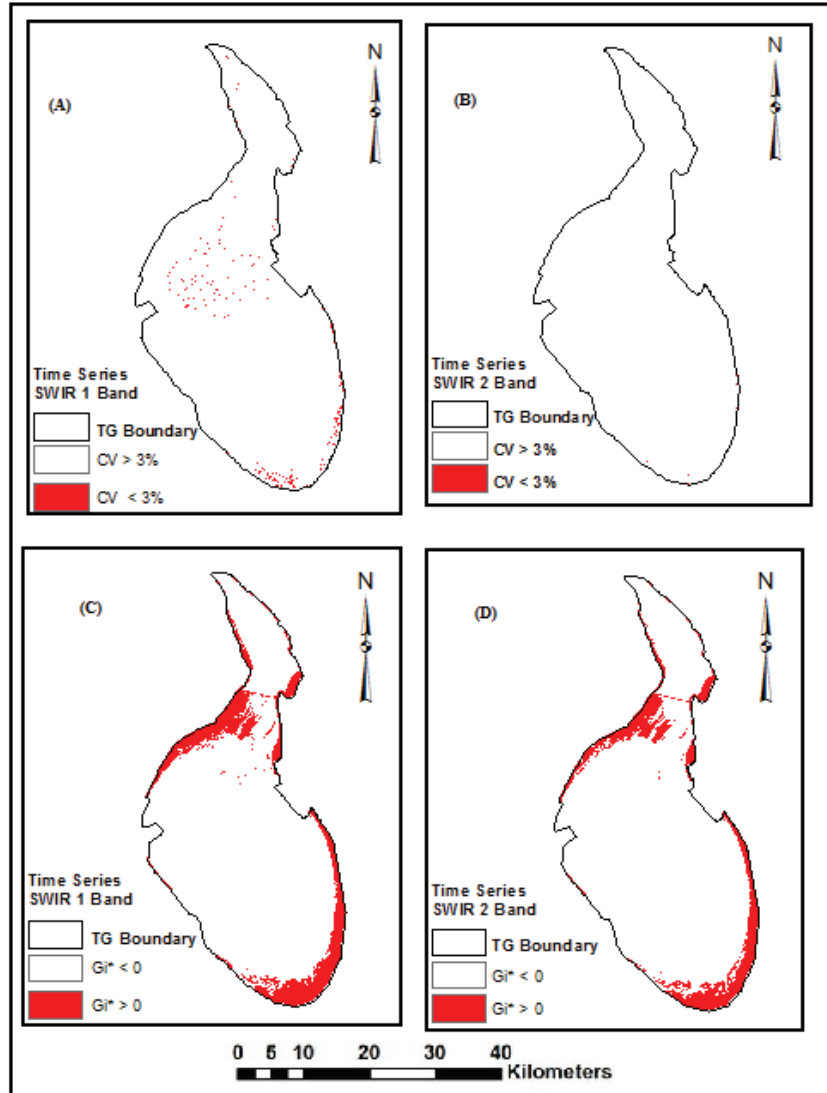
Figure 5.23: Time Series CV and Getis index maps of Tuz Gölü showing Landsat TM SWIR1(band 5) and SWIR 2 (band 7) at 30 m pixel resolution for the month August comprising of years 1984, 1985, 1987, 1989, 1998, 2003, 2007, 2009 and 2010.
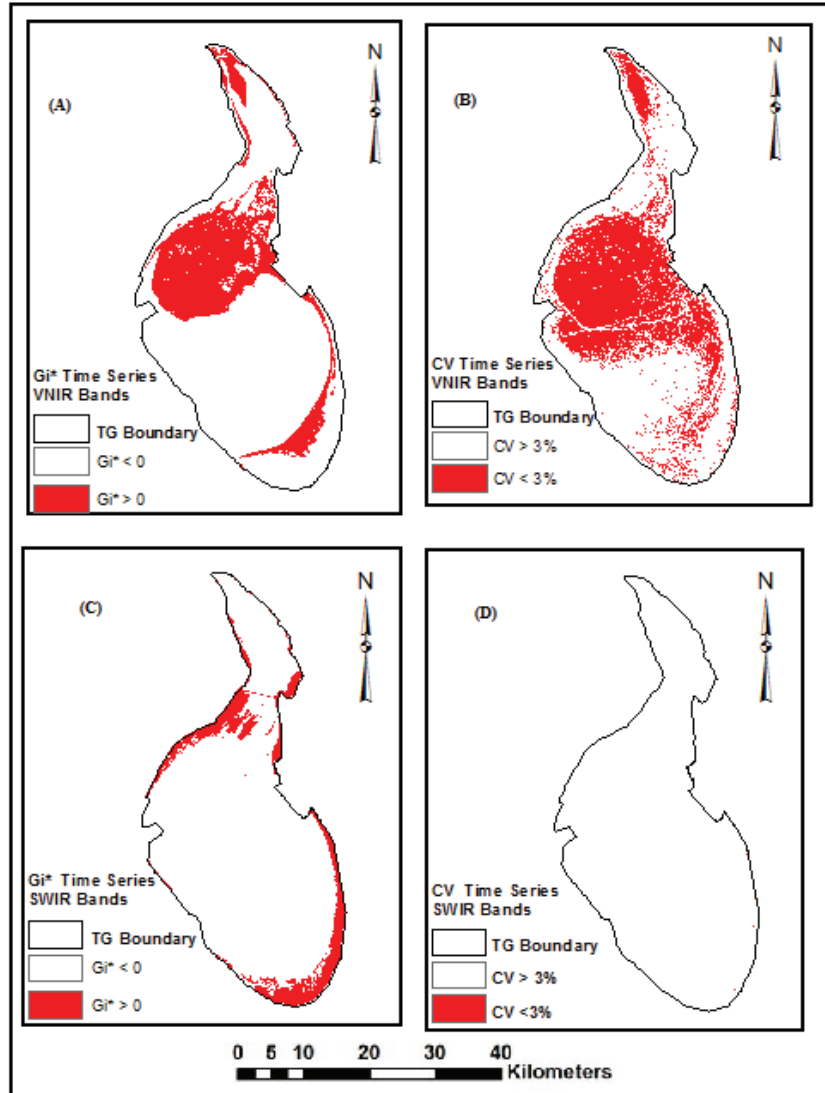
Figure 5.24: Time Series CV (CV < 3%) and Getis (Gi*> 0) index maps of Tuz Gölü showing Landsat TM VNIR [(A) & (B)] and SWIR [(C) & (D)] bands at 30 m pixel resolution for the month August comprising of years 1984, 1985, 1987, 1989, 1998, 2003, 2007, 2009 and 2010.

5.4.2. Comparing coefficient of variation assessment using different window sizes across Tuz Gölü

Figure 5.25 explains the effect of varying windows sizes (i.e. from small to large ones) used on computation of CV across Tuz Gölü. It was observed that much variation across the site was evident with respect to the use of localised window size (3×3) as compared to 5×5, 7×7 and 9×9 window sizes. This is closely linked to understanding the spatial structure of GCTs which was geared towards answering research questions 6 mentioned in section 1.3.1.
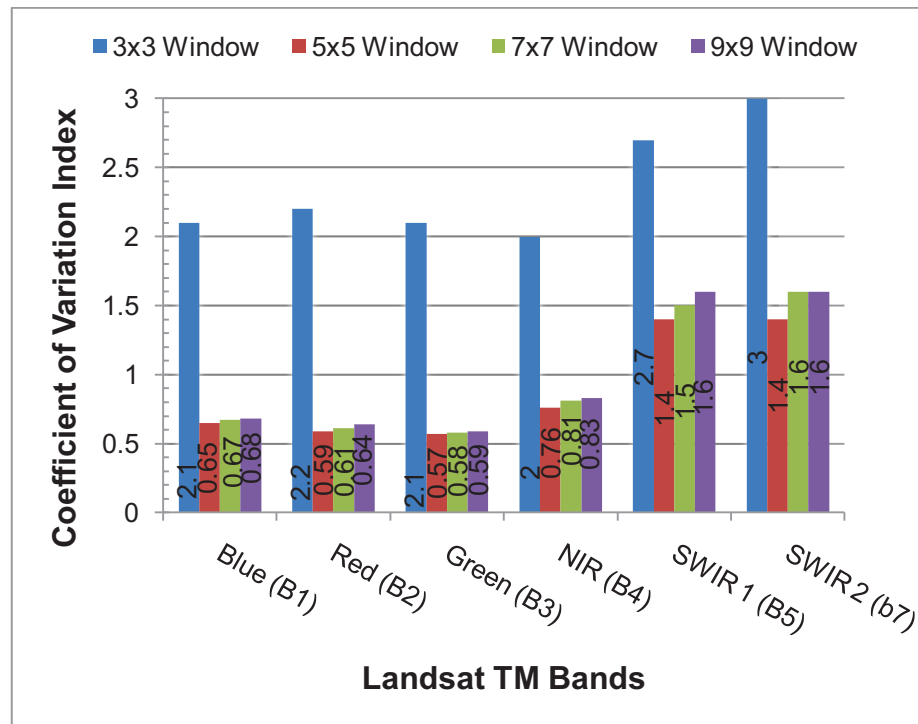
Figure 5.25: CV index range of Landsat TM VNIR and SWIR bands acquired over Tuz Gölü test site for 18/08/2010 image using different window kernels.

5.4.3. Spatial homogeneity analysis across Tuz Gölü: Combination Getis Ord statistic and CV Index

The identification of suitable spatial homogeneous areas within Tuz Gölü (TG) recommended for vicarious calibration and atmospheric activities was based on a criteria that combines Gi* statistic (i.e. Gi*> 0) and the CV (i.e. CV < 3%) to analyse the images (Figure 5.23 and 5.24, Appendix 11, 12).

The criteria is herein referred to as "Spatial homogeneity criteria" (SHC). In Figures 5.26, 5.27, 5.28 and 5.29, areas within Tuz Gölü that meet the set criteria are denoted by "Homogeneity". On the other hand, "Inhomogeneity" is used to denote areas that do not meet the set criteria for the Landsat TM, ASTER L1B and MODIS (MOD09A1) images.

Spatial homogeneity assessment using the set criteria for Tuz Gölü (TG) indicated that there is an expansive fairly homogenous and temporally stable areas concentrated at the middle of upper half of the lake respecting the VNIR bands of Landsat TM and ASTER at 30 m pixel resolution. This area was approximately 295 km^2 for the Landsat TM and 18 km^2 for the ASTER which constituted about 25% and 18% of the entire area of Tuz Gölü respectively. Smaller homogenous and temporally stable areas were also envisaged in the southern and northern parts at the fringes of the lake. These areas were of lesser extent compared to those found at upper middle part (Figure 5.26).

The results obtained for the MODIS Red & NIR, VNIR and SWIR bands at 480 m resolution are quite interesting. A larger area within TG (approximately 95%) was found to be homogeneous and temporally stable across SWIR bands for month of August for years 2004 – 2006. The extent of this observation is from north to south across the lake. The south western portion together with smaller portions of the upper north and the fringes of the TG constituting approximately 5% of the Lake's total areas were characterized by "inhomogeneity" across the MODIS SWIR bands (Figure 5. 29).

On the other hand, a considerable area(approximately 55%) in the north, middle portion, south and along the periphery of TG were found to be homogeneous and temporally stable across MODIS Red & NIR and VNIR bands for month of August for years 2004 – 2006. The middle portion together with smaller portions of the upper north and the fringes of the TG constituting approximately 45% of the Lake's total areas were characterized by "inhomogeneity" across the MODIS Red & NIR and VNIR bands (Figure 5. 29).
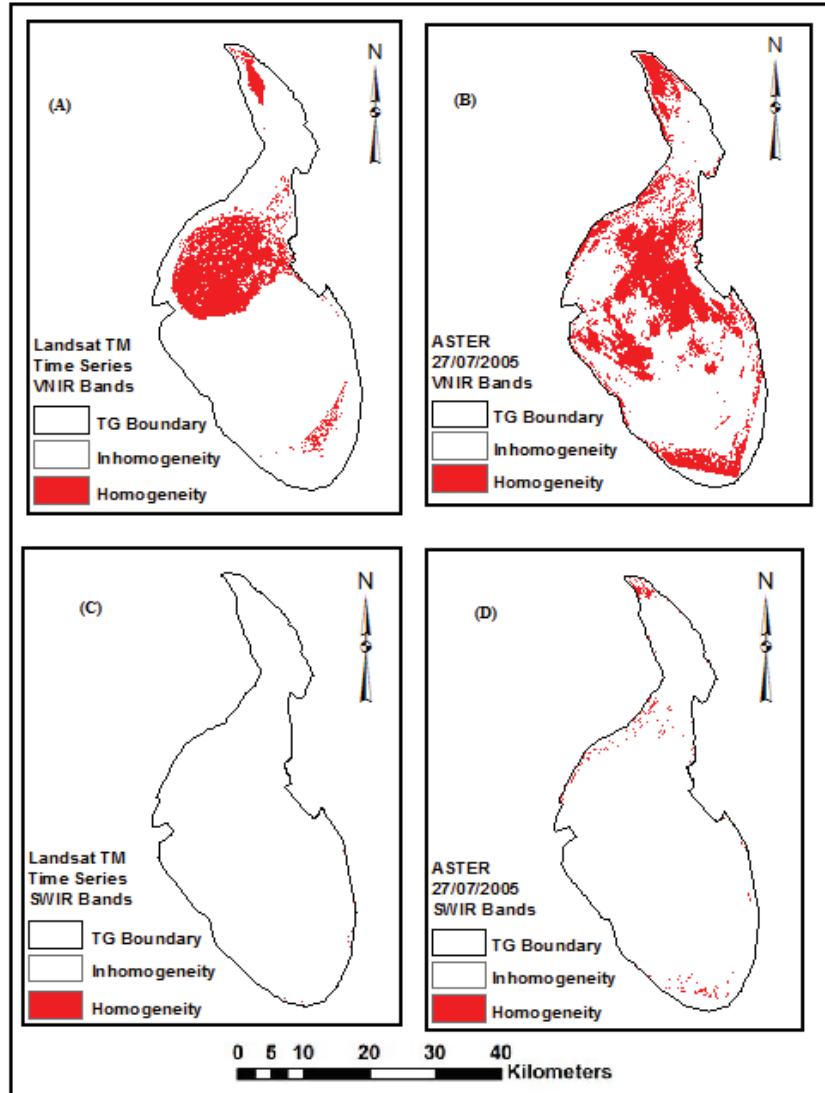
Figure 5.26: Spatial homogeneity criteria maps of Tuz Gölü showing Landsat TM and ASTER L1B VNIR [(A) & (B)] and SWIR [(C) & (D)] bands at 30 m pixel resolution for the month August comprising of years 1984, 1985, 1987, 1989,1998, 2003, 2007, 2009 & 2010 and July, 2005 respectively.
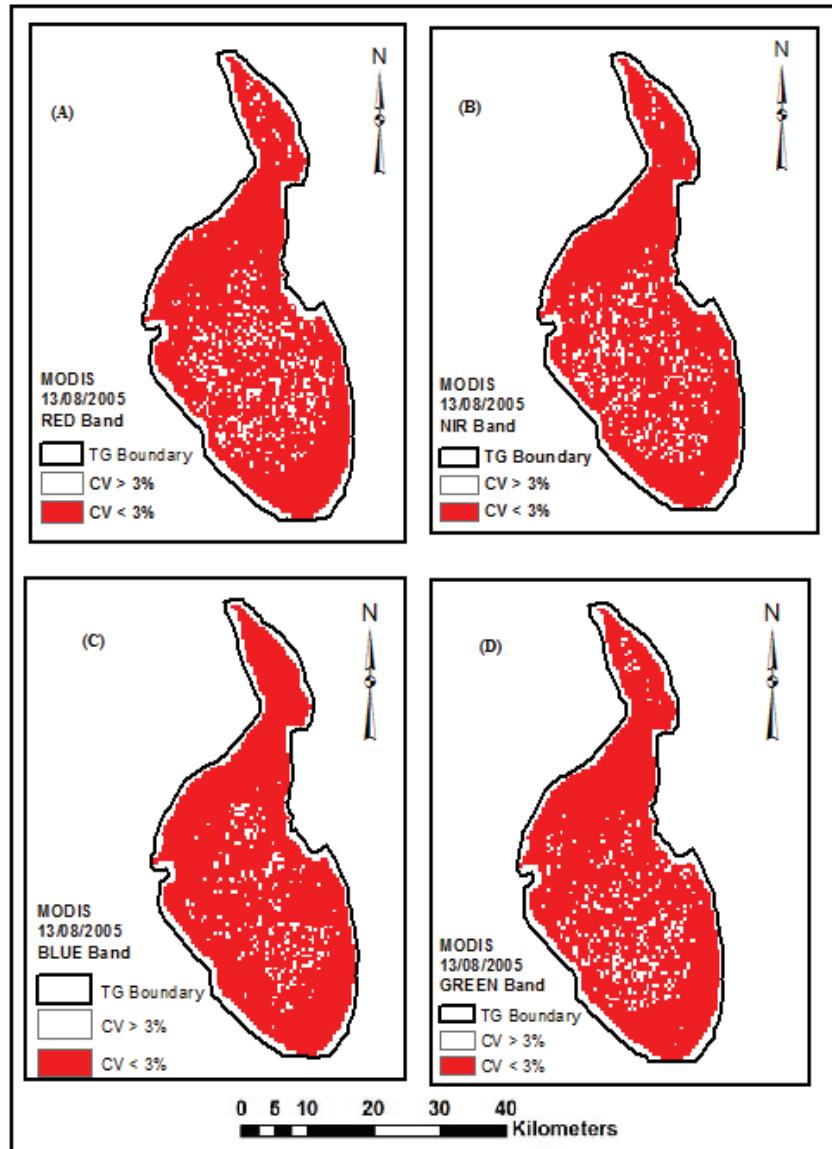
Figure 5.27: CV (%) index map of Tuz Gölü showing MODIS (MOD09A1) VNIR bands at 480 m pixel resolution for the month of August 2005.
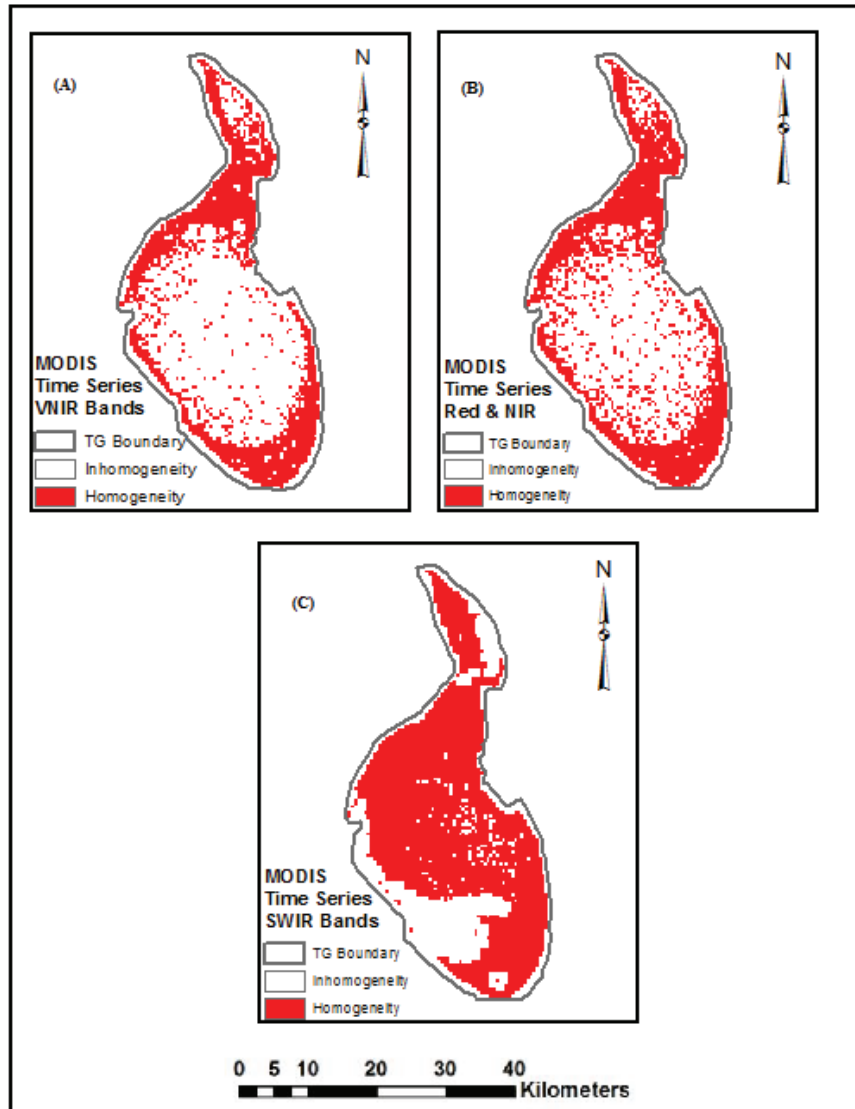
Figure 5.28: Spatial homogeneity criteria maps of Tuz Gölü showing MODIS (MOD09A1) VNIR, Red & NIR [(A) & (B)] and SWIR (C) bands at 480m pixel resolution for the month August comprising of years 2004 (2 images), 2005 (2 images) and 2006 (2 images).

5.4.4. Comparing Identified Spatial Homogeneous areas within Tuz Gölü based on different years combination.
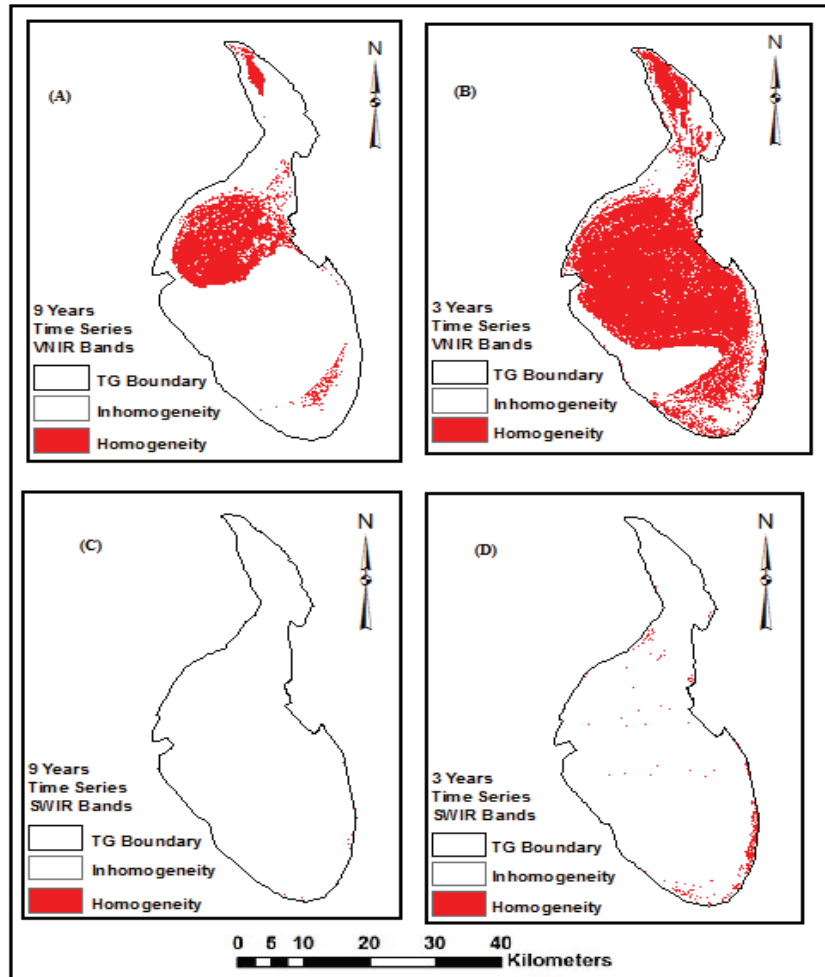
Figure 5.29: Spatial Homogeneity criteria maps of Tuz Gölü showing Landsat TM VNIR and SWIR in time series of 9years [(A) & (C)] and 3years [(B) & (D)].

In Figure 5.29, the result for the 9 years time series consist of a combination of images for the year 1984, 1985, 1987, 1989, 1998, 2003, 2007, 2009 and 2010 whilst the 3 years is a combination of year 2007,2009 and 2010 respectively. This result closely linked to understanding the spatial structure of GCTs which was geared towards answering research question 4 mentioned in section 1.3.1.

5.4.5.   **Comparing identified spatial homogeneous areas within Tuz Gölü across the VNIR and SWIR bands of Landsat TM and MODIS at 480m pixel resolution.**
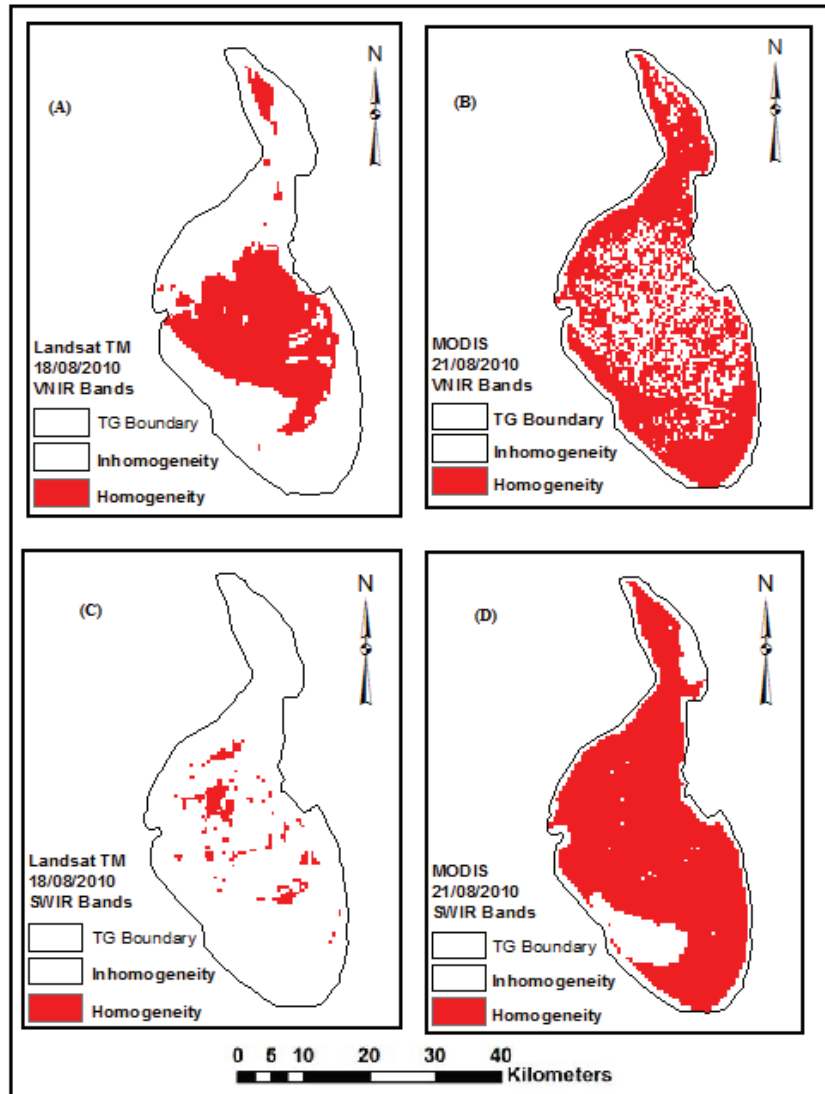
Figure 5.30: Spatial homogeneity criteria maps of Tuz Gölü showing Landsat TM and MODIS VNIR and SWIR at 480m pixel resolution. The Landsat TM and MODIS images used were captured on 18/08/2010 and 21/08/2010 respectively.

5.4.6. **Comparing identified spatial homogeneous areas within Tuz Gölü at different pixel resolutions (30 m, 240m, 480m and 1000m).**
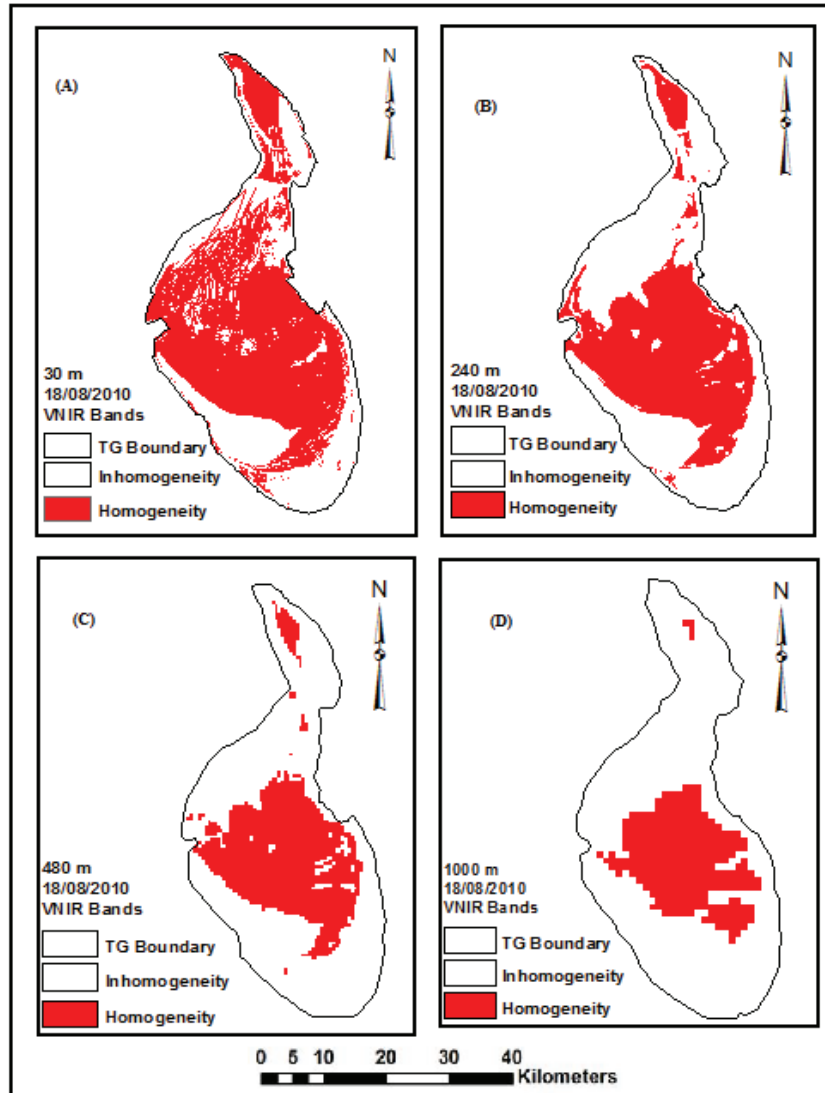
Figure 5.31: Spatial Homogeneity criteria maps of Tuz Gölü showing Landsat TM VNIR at (A) 30m, (B) 240m, (C) 480m and (D) 1000m pixel resolution of August, 2010.
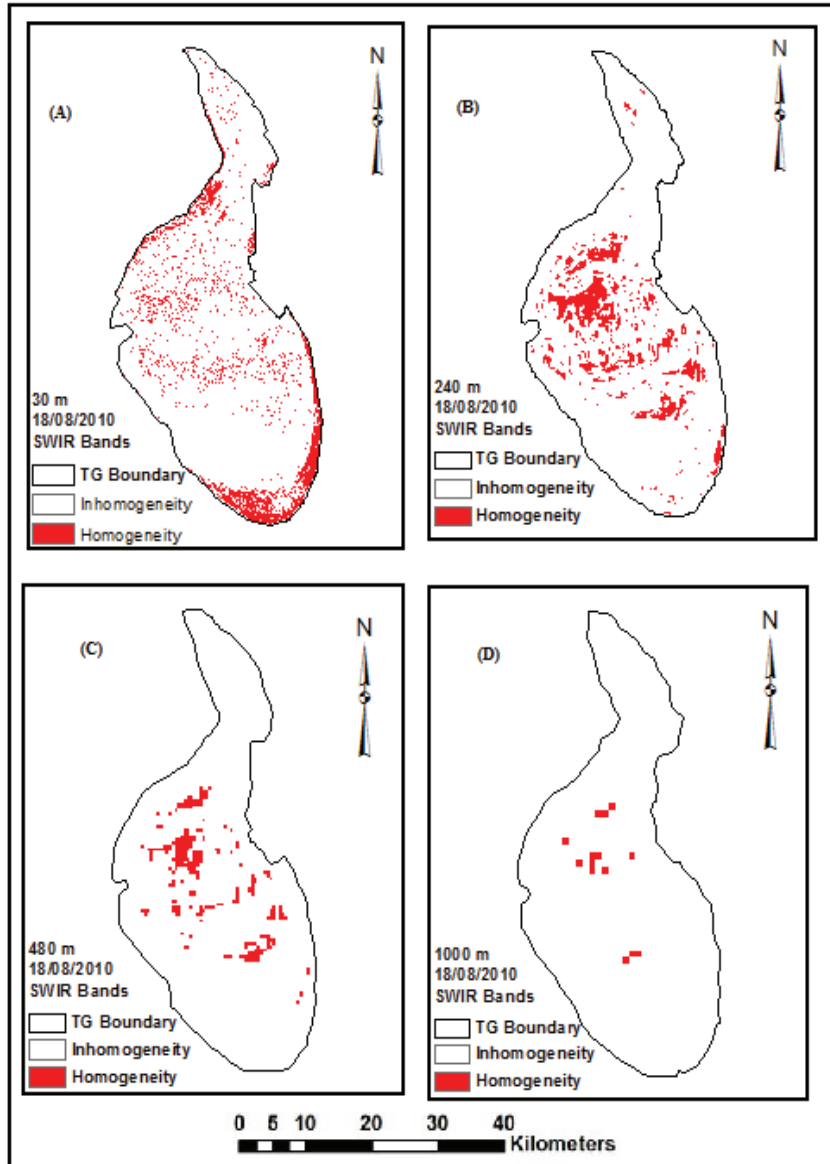
Figure 5.32: Spatial homogeneity criteria maps of Tuz Gölü showing Landsat TM SWIR at (A) 30 m, (B) 240m, (C) 480m and (D) 1000m pixel resolution of August, 2010.

In Figure 5.30, the spatial homogeneity assessment using SHC for Tuz Gölü (TG) indicates that there is an expansive fairly(approximately 45% of the entire Lake's area) homogenous and temporally stable area concentrated at the centre of the lake using the VNIR bands of Landsat TM. Comparatively, a larger area within TG (approximately 80%) was found to be homogeneous and temporally stable across the MODIS VNIR extending from north to south across TG. Few patches located in the middle of TG (approximately 5%) were found to homogenous and temporally stable respecting the Landsat TM SWIR bands at 480 m. Comparatively, a larger area within TG (approximately 75%) was found to be homogeneous and temporally stable across MODIS SWIR bands. This can be attributed to the larger area of CV < 3% and Gi* > 0 found for the MODIS VNIR and SWIR bands (see: Appendix 5 and 6) in comparison to the Landsat TM VNIR and SWIR bands at 480 m.

In Figures 5.31 and 5.32, it was observed that the area identified to be homogeneous and temporally stable tends to decreases gradually with increasing pixel resolution (i.e. from fine to coarser resolution) within a localised window size (3×3). This was observed across both the VNIR and SWIR bands of Landsat TM.

5.4.7. Identification of proposed sample site within TG for VC or AC activities

A surface was considered temporally stable when the CV within the local window was less than 3% as recommended by Teillet et al., (2007). Also such surfaces are to be spatially homogeneous with Gi* > 0 as recommended by Bannari (2005). Therefore, surfaces conforming to the above mentioned criteria are characterised to be potentially useful sites for vicarious calibration and atmospheric activities. Temporally stable areas within the identified spatially homogeneous areas of TG based on CV computations depicts that a majority (approximately 85%) of temporally stable areas fall within Gi* > 0 areas as shown in Figure 5.33.

The identification of the temporally stable areas over the spatially homogeneous area (having brighter pixel value/high reflectance) is crucial to sampling on the ground potential areas useful for vicarious calibration. Proposed site for VC and AC activities is located at the middle of the upper half of TG (Figure 5.34). These results gave insight into understanding the spatial structure of GCTs which was geared towards answering research questions 5 mentioned in section 1.3.1.

In this current study, the identified SHC area for Landsat TM VNIR bands is fairly similar (in terms of location and size) to the identified area found by Odongo (2010) using Landsat TM VNIR bands images captured in August, 1984,1989,2000, 2003, 2006 and 2009 (see: appendix 10). The identified SHC area constituted approximately 25% of the total area of Tuz Gölü in both this current study and the

study by Odongo (2010). However, this study identified a fairly large area (approximately 1400 m × 800 m) as proposed site for VC activities in comparison to an area of 885 m × 440 m identified by Odongo (2010). Comparatively, this could be attributed to the approach of masking of Tuz Gölü out of its surroundings, implying that Gi* and CV computation were confined to only Tuz Gölü surface with fairly uniform brighter reflectance values across the VNIR bands. Thus, a small global mean was used for computation in this current study. Whilst Odongo (2010) on the other hand, made use Tuz Gölü and its surroundings, meaning that CV and Gi* computations were carried out on images made up of two or more surfaces with low and high reflectance values across the VNIR bands. Thus, a large global mean was used for Odongo (2010) computation.
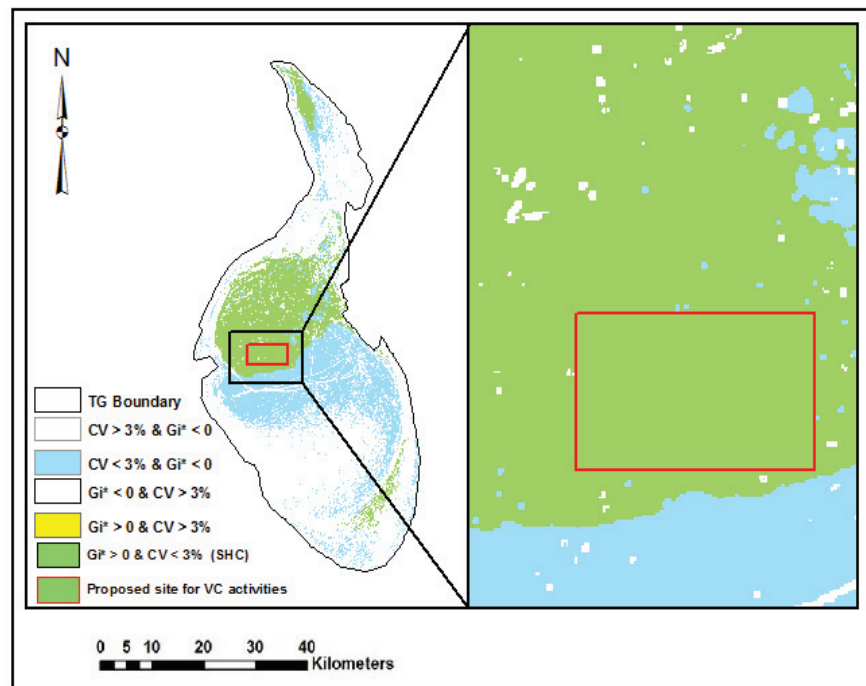
Figure 5.33: Spatio-temporal stability map for TG showing a selected proposed calibration site with respect to Landsat TM VNIR bands at 30 m pixel resolution for the month August for of years 1984, 1985, 1987, 1989, 1998, 2003, 2007, 2009 & 2010. Where: SHC means Spatial Homogeneity Criteria.

6. DISCUSSION

6.1. Characterizing the spatial structure of GCTs: Tuz Gölü site

A pattern of increment in reflectance ($\times$ 4%) was evident in the northwest to southeast direction with respect to the Green, Red and NIR bands of Landsat TM (Figure 5.5). Also, a similar pattern of increment in reflectance ($\times$ 4%) was observed in the north to south direction from a distance of 1.5 km to 4.5 km (Figure 5.2). The observed trend in reflectance ($\times$ 4%) across the spatial structure of TG will play an important role in selecting homogeneous patches with higher reflectance within the entire areas during calibration and validation activities in the field. This is due to the fact that vicarious calibration requires homogeneous surfaces reflectance factor greater than 0.3 (Thome, 2001;Kneubühler et al., 2006;Teillet et al., 2007).

The variograms were useful in characterize the spatial autocorrelation structure of TG as a function of the ground scene and the Landsat TM parameters (Woodcock et al., 1988) . In Figures 5.6 - 5.11, it is evident that pixel values that are at close distant apart will have strong spatial autocorrelation than pixel values which are far from each other (Spiker and Warmer, 2007). The observation of two different levels of autocorrelation structures (i.e. short and long range) across Landsat TM VNIR and SWIR bands suggests that two forms of surfaces with respect to the distribution of reflectance (HDRF) can be found within TG. These imply that, selection of surfaces within TG for VC activities should not be at wider distance apart in order to achieve existence of homogeneity in the selected surfaces and thus ensuring consistency in measured reflectance values.

Geary's C Index was useful in characterizing spatial autocorrelation observed across Tuz Gölü. Understanding the spatial structure of surfaces plays an important role in sampling design techniques. The spatial autocorrelation of the dataset (across the Tuz Gölü Lake) is stronger in the visible bands compared to that of the infrared and SWIR bands (Figure 5.12). This implies that Landsat TM VNIR bands at 30 m resolution are more reliable and will exhibit homogeneity in measured reflectance values in comparison to the SWIR bands. Hence, the Landsat TM VNIR is recommended for vicarious calibration activities when using TG site. Similar observations are discussed in the works of Gurol et al, (2008) and Odongo (2010) concerning the Landsat TM VNIR bands. The higher spatial variation occurrence in the SWIR band may be attributed to spatial dynamic changes that might occur in ground calibration target surfaces due to changes in surface moisture, deposition of metals such as iron, gypsum and magnesium on the surface, presence of vegetation (Kneubühler et al., 2006) and also the mineralogy (Magee, 1991) of the site that may possibly introduce variation on the surface. These changes may vary seasonally

causing significant variation of spectra, and therefore, render those surfaces less worthwhile for VC or AC campaigns.

6.2. Spatial autocorrelation analysis and comparison of VNIR and SWIR bands of Landsat TM and MODIS (MOD09A1) at 480m pixel resolution

It can be inferred from Figure 5.13 - 5.18 that, the VNIR bands of Landsat TM and MODIS (MOD09A1) exhibit a similar spatial autocorrelation pattern (using Geary's C indexing) of Tuz Gölü site in comparison to the SWIR bands. Thus, some areas of Tuz Gölü will correlate more in the VNIR bands but not in the SWIR bands of both sensors at 480 m pixel resolution. This also indicates that the two sensors (Landsat TM and MODIS) may be comparable within the VNIR region of the spectrum in examining spatial homogeneity property of Tuz Gölü site. Comparatively, a larger area within TG (approximately 80%) was found to be homogeneous and temporally stable across the MODIS VNIR extending from north to south across TG. Few patches located in the middle of TG (approximately 5%) were found to homogenous and temporally stable respecting the Landsat TM SWIR bands at 480 m. This will be useful during the calibration and validation of the two satellite sensors at similar resolutions respecting the usage of Tuz Gölü as the reference site

The spatial autocorrelation observed using the Geary's C index for the VNIR and SWIR bands of Landsat TM and MODIS (MOD09A1) were evident in the identified SHC areas across the VNIR and SWIR bands of the two sensors at 480 m pixel resolutions. In Figure 5.30, using SHC for Tuz Gölü, comparable homogenous and temporally stable area which was concentrated at the centre of the lake (approximately 45% of the entire Lake's area) was found across both Landsat TM and MODIS VNIR bands at 480 m pixel resolution. However, a larger area within TG (approximately 75%) was found to be homogeneous and temporally stable across MODIS SWIR bands than that of Landsat TM SWIR. This can be attributed to the larger area of CV < 3% and Gi* > 0 found for the MODIS VNIR and SWIR bands (see: Appendix 5 and 6) in comparison to the Landsat TM VNIR and SWIR bands at 480 m.

6.3. Effect of varying window sizes on spatial homogeneity and temporal stability assessment of GCTs

Based on the recommendation made by Bannari et al., (2005), Kneubuhler et al., (2006) and Teillet et al., (2007), temporally stable areas suitable for vicarious activities were identified within Tuz Gölü across the VNIR and SWIR bands of Landsat TM (Figure 17, 20, 5.20 and 5.21). An area of approximately 80% of within Tuz Gölü was identified to be temporal stable across the VNIR bands (appendix 10). The low CV value (CV < 3%) obtained for the identified temporal stable areas

across the VNIR bands within Tuz Gölü is an indication of a good temporal stable site. Also, the low CV recordings in the NIR depicts that the site is devoid of vegetation (Figure 5.20).

A small window size (3×3) depicts that the spatial dependency among the dataset is confined to a much localized regions. A large window on the other hand depicts that the spatial dependency is viewed within a wide region (Bannari et al., 2005). The results obtained indicated that small window size (3×3) highlights more of the variation across the surface across all the bands in comparison the medium (5×5) and large (7×7 and 9×9) window sizes (Figure 5.25). This implies that CV computations based on small window size are much localized with respect to spatial dependency within the datasets whilst the opposite is true for large windows. Thus, in this study, the small window (3×3) was considered appropriate for the spatial homogeneity assessment of Tuz Gölü.

6.4. Comparing identified spatial homogeneity areas and effect of different years combination

Spatially homogeneous areas within Tuz Gölü were identified across the VNIR and SWIR bands of Landsat TM, MODIS and ASTER satellite images employed in this study based on SHC. The results obtained depict that there are areas, which are homogeneous and temporally stable over time (i.e. year-by-year) in Tuz Gölü across the VNIR bands. These homogeneous and temporally stable patches are known to characteristically clustered into typical salt pans and playa (Earl, 1990). Possibly, these groupings could be due to sub-environments identifiable facies which aggregate into salt crusts usually formed in the centre of playas (Magee, 1991).

It was also evident that much of the area within TG (an estimate of 70 to 75%) is more variable and not all of it is stable year after year with respect to the Landsat TM and ASTER VNIR bands respectively. The occurrence of such situation may be attributed to the ephemeral nature (seasonality of the salt lake) of TG where it experiences intra-annual and inter-annual variations in the surface. These variations could be responsible for the modification of the surface structure properties (Ledrew et al., 2004; Ledrew and Lim, 2005). A larger area within TG (approximately 98%) was found to be more variable for the ASTER and LTM SWIR bands respectively. This implies that almost the entire area was not stable over time for the Landsat TM and ASTER SWIR bands. This suggests the unsuitability in using the SWIR bands of ASTER and Landsat TM for vicarious calibration and atmospheric correction activities respecting TG site.

The results depict that combining more images (for instance 8 years) over time gives an output with smaller identified homogeneous and temporally stable areas

across the VNIR and SWIR bands of Landsat TM (Figure 5.26). The opposite was also found true when few images (for instance 3 years) are combined over time. This implies that the extent of the identified homogeneous and temporally stable areas across the TG site tends to decrease over time. However, this may be subjective and may depend primarily on the changes in the prevailing environmental and climatic conditions (Kneubühler et al., 2006; Gurol et al., 2008) of the site from year to year. For instance, drier years may result in identification of large areas of Tuz Gölü to be spatially homogeneous and temporally stable in comparison to wet years. Thus, it will be useful to access the linkage of the prevailing weather conditions with the identified spatial homogeneous areas.

The observation of a larger homogeneous and temporally stable area across MODIS SWIR bands in comparison to its Red & NIR and VNIR bands (Figure 5.25) can be attributed to the difference in the areas identified to be temporally stable (i.e. areas within TG that meet the criterion CV < 3%) (See: appendix 13).

6.5.   Comparison of spatial homogeneity criteria at different pixel resolution

Comparatively, small patches were identified to be temporally stable at coarse resolution than at fine resolution. This may have led to the difference in the extent of areas identified to be spatially homogeneous (having brighter pixel/reflectance values) and temporally stable based SHC. Also, across board (i.e. from fine to coarse resolution) a large area within TG was found to be spatially homogeneous (having brighter pixel/reflectance values) and temporally stable for the VNIR bands as compared to the SWIR bands. Inference from Figures 5.28 and 5.29 indicates that there exists higher spatial correlation at shorter lags (Spiker and Warmer, 2007). Knowledge about the spatial homogeneity extent of Tuz Gölü 's structure with respect to varying pixel resolution (i.e. from fine to coarse) will be useful in determining which satellite sensor type is most appropriate in designing sampling techniques for selecting homogeneous patches within the entire areas for calibration and validation activities.

6.6.   Characterizing spatial homogeneity and temporal stability of Tuz Gölü

Spatial homogeneity of a test site can be affected by different factors including surface moisture, variation in topography creating shade effects, and vegetation which may cause changes in spectral measurements (Kneubühler et al., 2006). Tuz Gölü being an ephemeral lake, it was expected that there will be variation in the moisture conditions of the lake year to year. This will affect the spatial homogeneity and temporal stability of the site.

Generally, most studies that involve the characterization of spatial homogeneity and temporal stability properties of a GCT surface had used only coefficient of variation (CV) as a measure of the two properties (Scott et al., 1996; Cosnefroy et al., 1996; Kneubühler et al., 2006). This has resulted in the impression that these properties are one and for that matter the same thing. A fact that Cosnefory et al., (1996) approved and documented saying *"...for reasons of practicability, we have chosen to privilege the spatial uniformity criterion, conjecturing that if a site is repeatedly very uniform over a large period of time, it is quite likely that it should satisfy the other criterion as well"*. The "*other criterion*" used here refers to temporal stability.

However current studies indicate otherwise as in case of the works by Bannari et al., (2005), Gurol et al., (2008) and Odongo (2010) where the authors demonstrated that a surface could be repeatedly spatially homogeneous over time but not necessarily temporally stable for vicarious calibration campaign.

In this study, these two properties were defined and evaluated separately but much emphasis was placed on the spatial homogeneity property of GCTs which the focal point of this study. Evidently, the results obtained implies that the identified temporally stable and spatially homogeneous area is located at the upper central part of Tuz Gölü year after year (Figure 5.32).The identified proposed site within TG with respect to the VNIR bands (Figure 5.32) as found to be located in the upper half of TG confirms a similar observation made by Odongo (2010) using Landsat TM images but in contrast to the findings made by Pegrum (2008) using MODIS images (see: Appendix 10). This identified area was approximately 1400 m × 800 m in size. Comparatively, the identified proposed site is three times the size of La Crau test site in France and Rail Road Playa Valley (RRPV) in US. Whilst Odongo (2010) identified an area of approximately two times the size of La Crau test site in France and Rail Road Playa Valley (RRPV) in US. The identified consistently homogeneous patch also has brighter pixels (HDRF) which are significant for vicarious calibration and atmospheric correction campaigns.

The observed spatially homogeneous and temporally stables areas (Figure 5.26) across the Landsat TM VNIR and SWIR bands suggests that SWIR bands may not be suitable for vicarious calibration and atmospheric correction campaigns respecting TG site. This due to the fact that the SWIR bands were devoid of consistently homogeneous patch through time and also had HDRF values fairly below the recommended greater than 0.3 [i.e. a value of 120 in the case of reflectance (× 4%)] as stated in point number 2 of section 2.1.

It was evident that CV computed within a local window can be misleading in interpreting spatial homogeneity. This is due to the fact that two adjacent surfaces may have equal CV but have different means and standard deviations altogether.

Furthermore, a CV computed within a local window may itself vary across years for the same local window (compare Figure 5.22 and Appendix 8). Hence, an index that best evaluates change in spatial homogeneity of a VC site was adopted (i.e. combination of Gi* and CV) to characterize spatial homogeneity of TG site. It is worth noting that spatial homogeneity do exhibit some form of temporal dimension, in that there may be patches, which may progressively shift from being homogenous to heterogeneous and vice versa from year to year (Ledrew et al., 2004; Ledrew and Lim, 2005). Moreover, the results of spatial homogeneity assessment reveal that there were some areas within Tuz Gölü that were actually homogeneous but not temporally stable. This implies that application of the CV alone to account for spatial homogeneous and temporal stability as argued by Cosnefory et al., (1996) would lead to wrong characterization of the surface.

It is necessary that homogeneity assessment be upheld across all bands of the sensor and from year to year respecting VC campaigns. The CV can then be used to determine temporal stability by computing the variability in spectra retrieved from images. This will contribute greatly in guaranteeing the spatial homogeneity and temporal integrity of a test site. This technique provide for the use of spatial statistics as a quality metric for characterizing HDRF of GCTs on a spatial scale. Granted, the actual CV measurement of a test site may change over time due to prevailing environmental and climatic conditions (Kneubühler et al., 2006). However, as long as the changes in the actual CV value of the test site does not exceed the recommended threshold of CV < 3% (Teillet et al., 2007), such site are considered temporally stable and potentially useful for vicarious calibration campaigns. Moreover, this implies that variation in HDRF measurements can be envisaged over time even though such surfaces (especially adjacent surfaces) may have a similar CV value of less than 3% through time.

A preliminary study in characterizing Tuz Gölü by National Physics Laboratory (NPL) of United Kingdom employed Getis Ord* statistic as a measure of both spatial homogeneity and temporal stability of the site (Pegrum, 2008; Gurol et al., 2008). Their studies excluded the computation of variation in HDRF using coefficient of variation method. However, the application of Gi* alone to account for spatial homogeneity and temporal stability as argued by Bannari et al., (2005) could misinform on the true characterization of a surface's stability through time. Furthermore, their study only made used of the red and near infra bands of MODIS imagery from 2006 to 2008 for the months of July and August to characterize for spatial homogeneity of Tuz Gölü. Odongo (2010) on the other hand, did account for both spatial homogeneity and temporal stability of the site by applying Gi* and CV to Tuz Gölü and its surroundings. His work focused on Landsat TM VNIR bands.

The current study also used a combination of Gi* and CV similar to that of Odongo (2010), but the computations were carried out only on Tuz Gölü by masking its surroundings. The identified spatial homogeneous areas by these authors were quite different from the one found in this study (compare Figure 5.32 and Appendix 10) especially that of Gurol et al., (2010) and Pegrum (2008). Comparatively, a much wider area (approximately 1400 m x 800 m) was identified to be spatially homogeneous and temporally stable for VC campaigns in the current study than (885 m x 440 m) found by Odongo (2010) but had similar location. This can be attributed to their methodological approach, which was different from that outlined in the present study. The methodological approach of masking Tuz Gölü as employed this study is preferred to using an imagery of Tuz Gölü together with its surroundings as demonstrated by Odongo (2010), Gurol et al., (2010) and Pegrum (2008). This is because, in the former, CV and Gi* computations are restricted to only Tuz Gölü as a single surface having high reflectance values and thus eliminate the effects of Tuz Gölü's surroundings on the resulting CV and Gi* values. Whilst in the latter, CV and Gi* computations will be carried out on two or more surfaces having low and high reflectance values and may influence the resulting CV and Gi* values.

The current study defined homogenous and bright pixels (Gi* > 0) of the study area from ten Landsat TM imagery dataset for bands 1, 2, 3, 4, 5 and 7. Then temporally stable (CV < 3%) areas were identified from nine satellite imagery datasets, which were overlaid on the homogenous and bright pixels layer. The output map represent areas which were spatially homogeneous and temporally stable to within 3% for VNIR bands (Figure 5.32) as recommended for vicarious calibration test sites (Biggar et al., 1994; Thome et al., 1997).

Gi* statistic has been used in vegetation cover classification (Wulder and Boots, 1998) and currently applied in identifying spatial homogeneity of vicarious calibration sites (Bannari et al., 2005; Gurol et al., 2008; Odongo, 2010). Bannari et al., (2005) applied Gi* and CV as a synergistic procedure to characterize the spatial homogeneity and temporal stability of Lunar lake playa in Nevada, US. The authors used SPOT HRV spectral bands 1, 2, and 3 for March 1997, June 1997 and June 1998. Bannari et al. (2005) showed that, the two indices combined give a better characterization of the spatial homogeneity and temporal stability of calibration sites and thus provided a new approach to the use of spatial statistics as a quality metric to characterize vicarious calibration test sites.

6.7. Importance of method of measurement to vicarious calibration

VC campaigns play a crucial role in guaranteeing that data products from Earth observation (EO) sensors are of high quality. This implies that, the measurements of inputs (i.e. reflectance of ground calibration targets and environmental variables: aerosol loadings) employed in these activities should have a high accuracy. This will minimize inherent uncertainties/errors during estimating inputs which are transferrable to the sensor from propagating into the resulting EO products (Biggar et al., 1994; Thome et al., 1998). These levels of uncertainty have much implication on the use of EO products applications. For instance, in studying subtle changes of the Earth such as climate monitoring (Pinty et al., 2005; National Physical Laboratory, 2010) and several vegetation indices (VI) (Miura et al., 2000).

Miura et al., (2000) demonstrated that the impact of reflectance calibration uncertainties influence the accuracies of V1 using MODIS sensor onboard the TERRA platform. The authors observed that VI uncertainties tend to decrease when the calibration errors were positively correlated between MODIS bands. Miura et al., (2000) in using field observational canopy reflectance data found a mean VI uncertainties of approximately 0.01 VI units for the normalized difference vegetation index (NDVI) and the soil-adjusted vegetation index (SAVI) and 0.02 VI units for the atmospherically-resistant vegetation index (ARVI) and EVI under normal atmosphere conditions (i.e. greater than or equal to 20 km visibility) for a 2% reflectance calibration uncertainty. In summary, Miura et al., (2000) reported that the magnitudes of the mean VI uncertainties due to sensor calibration were less than 0.02 of VI dynamic range and can be considered satisfactorily low.

Another study reported that the impact of TOA radiance uncertainties on the operational Medium Resolution Imaging Spectrometer (MERIS) Level 2 land fraction of absorbed photosynthetically active radiation (FAPAR) products accuracy is approximated in the range of 5–10% (Gobron et al., 2008) .

Climate change models are known to be sensitive to retrieved surface albedo, having accuracy range of ±0.02 to ±0.05 deemed as appropriate (Sellers, 1995; Oleson et al., 2003). Also retrieval of aerosol optical thickness (AOT) for AC algorithms is known to be sensitive to measured surface HDRF (Guoyong et al., 1999). They explained that uncertainties associated with reflectance (HDRF) measurements may propagate gradually into errors associated with AOT retrieval. This will have a great impact on AC algorithms, which in turn used in correcting atmospheric effect and retrieve at-sensor reflectance products. Therefore, it is always necessary to have prior knowledge with respect to the degree of error or accuracy associated with a particular EO product before their usage. This also suggests that, the methods used in characterizing GCTs should account for errors involved and well documented.

7.   CONCLUSIONS AND RECOMMENDATIONS

A well characterized GCT with regards to its spatial homogeneity and temporal stability properties is crucial to the quantification of errors/uncertainties associated with satellite sensors post-launch. Errors resulting from VC campaigns are transferable throughout the lifespan a sensor and can seriously generate uncertainties in the sensor's derived products. These, in turn, will make decision making always challenging. The dynamic nature of many apparently stable surfaces is a major source of uncertainty/error due to the spatial heterogeneity of surfaces that appear homogeneous to naked eye.

This study sought to identify and investigate "spatial homogeneity" property of GCTs for a thorough understanding of their spatial structure. The study further aims at characterizing the influence of scale (pixel size and window size) measurements on spatial homogeneity property of GCTs by developing and testing methods for its assessment. To achieve the set objectives, the research questions defined in section 1.3.1 were properly answered:

What constitutes spatial homogeneity of ground calibration targets? Spatial homogeneity is viewed broadly as the state or characteristic of a surface to be made up of the same constituents in space. Spatial homogeneity simply entails the identification of areas/surfaces with similar reflectance values within an image. Thus, the spatial homogeneity of GCTs denotes homogeneity over an extended area of several pixels which is spectrally dependent.

How should spatial homogeneity of GCTs be measured? The spatial homogeneity property of GCTs is best characterized using both global and local autocorrelation measures (i.e. semi-variance, Geary's C index and Getis Ord*) together with CV. It is also important to mask out the area of interest. The variogram and correlogram were useful in exploring the spatial autocorrelation structure of HDRF across Tuz Gölü. Whilst a combination of Gi* (i.e. Gi* > 0) and CV (i.e. CV < 3%) characterize the identification of spatially homogeneous and temporally stable areas useful for vicarious calibration campaigns.

How does spatial homogeneity vary across the spectral bands [the visible, infra red and short-wave infrared (SWIR) portions of spectrum]? Local variation of HDRF measurements across the VNIR and SWIR bands were found to be dependent on the spatial homogeneity and temporal stability of a surface. An area that was spatially homogeneous, temporally stable and exhibited normal distribution in the VNIR spectra (approximately 1400 m x 800 m) was identified as a proposed VC site in Tuz Gölü, Turkey. Identification of such an area across the SWIR bands was not possible due to high variation and mineralogy of the site from a

geomorphologic view point. Also HDRF values of the SWIR bands were fairly below the recommended greater than 0.3 [i.e. a value of 120 in the case of reflectance (× 4%)] as stated in point number 2 of section 2.1.

Does the reflectance (HDRF) of GCT surfaces remains invariant across the VNIR and SWIR bands from year to year? Granted, a surface can remain spatially homogeneous and temporally stable through time. However, this was only true for across Landsat VNIR bands. The Landsat SWIR bands were devoid of such a site through time.

How does spatial homogeneity vary with pixel size? It was evident that identified spatial homogeneous and temporally stable areas within a localised 3×3 window tends to decrease from finer to coarser resolution across the VNIR and SWIR bands, possibly due to increasing variation in CV computation from finer to coarser resolution.

How does spatial homogeneity vary with window sizes used to assess spatial structure? A small window size (3×3) depicts that the spatial dependency among the dataset is confined to a much localized regions whilst large windows (5×5, 7×7 and 9×9) indicate that the spatial dependency is viewed within a wide region. Thus, the 3×3 window highlighted more of the variation across Tuz Gölü with values ranging from 0 to 3 across all the bands in comparison to the 5×5, 7×7 and 9×9 windows.

In summary, this study has attempted to characterize the spatial structure of a GCT by assessing its spatial homogeneity property across the VNIR and SWIR bands of Landsat TM, MODIS and ASTER at varying pixel resolution. It was perceived from this study that, the characterization of the atmosphere and the surface (i.e. spatial homogeneity and temporal stability) are crucial to VC campaigns. Nevertheless, the research still had some limitations due time constraint, absence field data (reflectance measurements) which would have been useful in correcting errors associated with HDRF values during the atmospheric correction procedure. Also, the unavailability of enough ASTER images in the months of July/August made it impossible to realise SHC areas across the ASTER VNIR and SWIR through.

7.1. Recommendations

This study focused on characterizing the spatial domain of GCTs through time across the VNIR and SWIR bands of Landsat TM, MODIS (MOD09A1) and ASTER L1B sensor which is a novelty of this study as an extension of a preliminary study conducted by Odongo (2010). The following recommendations highlight specifically on best practice guidelines that should be adopted when characterizing GCTs for VC and AC:

1. Spatial homogeneity and temporal stability of GCTs are two different properties of a surface and should not be considered to be the same. The general assumption that they are the same need to be tested to better inform on the nature of surfaces. The use of a combination of spatial statistic indices (e.g. Gi* and CV) as a quality metric will greatly enhance these characterization.

2. There is need to investigate the effect of moisture on natural GCTs HDRF measurements. Specifically, testing for a hypothesis on how soon the targets regain their actual HDRF after a rainfall event.

3. Beyond characterizing spatial homogeneity and temporal stability of a GCT surface, there is the need for interdisciplinary approach to fully understand the dynamic nature of GCTs especially in the SWIR bands.

4. Granted, the actual CV measurement of a test site may change over time due to prevailing environmental and climatic conditions (Kneubühler et al., 2006). Such site are considered temporally stable and potentially useful for vicarious calibration campaigns as long as the changes in the actual CV value of the test site does not exceed the recommended threshold of CV < 3% (Teillet et al., 2007). However, variation in HDRF measurements can be envisaged over time even though such surfaces (especially adjacent surfaces) may have a similar CV value of less than 3% through time. Thus, there is the need to query the CV as a classical measure in determining temporally stability of calibration site.

8. REFERENCES

ANDERSON, K. 2005. Temporal variability in calibration target reflectance: Methods, models and applications *Unpublished PhD thesis, University of Southampton, UK, 30 pp.*

ANDERSON, K. & MILTON, E., J., 2006. On the temporal stability of ground calibration targets: implications for the reproducibility of remote sensing methodologies *International Journal of Remote Sensing* 27**,** 3365-3374.

ANDERSON, K. & MILTON, E. J. 2005. Characterisation of the apparent reflectance of a concrete calibration surface over different time scales. In, Proceedings of the 9th International Symposium on Physical Measurements and Signatures in Remote Sensing (ISPMSRS) *Institute of Geographic Sciences and Natural Resources Research, CAS.*

BANNARI, A., OMARI, K., TEILLET, P. M. & FEDOSEJEVS, G. 2005. Potential of Getis Statistics to Characterize the Radiometric Uniformity and Stability of Test Sites Used for the Calibration of Earth Observation Sensors. *IEEE Transactions on Geoscience and Remote Sensing, 43(12): 2918-2926.*

BIGGAR, S. F., SLATER, P. N. & GELLMAN, D. I. 1994. Uncertainties in the in-flight calibration of sensors with reference to measured ground sites in the 0.4-1.1 m range. *Remote Sensing of Environment,* 48**,** 245-252.

BIGGAR, S. F., THOME, K. J. & WISNIEWSKI, W. 2003. Vicarious Radiometric Calibration of EO-1 Sensors by Reference to High-Reflectance Ground Targets. *IEEE Transactions on Geoscience and Remote Sensing, 41(6): 1174-1179.*

CEOS 2000. Improving the traceability to SI of the high level data products of Earth Observation (EO) measurements *6 pp, Available [online]: http://calvalportal.ceos.org/cvp/web/guest/cal/val-wiki/-/wiki/Main/Landnet (Accessed: 14 August, 2010).*

CEOS. 2010. *Template for information regarding the prime CEOS WGCV Cal/Val site for the post-launch characterization and calibration of optical sensors* [Online]. Available: http://calval.cr.usgs.gov/images/sites_catalog/Sites_Template.pdf [Accessed].

COSNEFROY, H., LEROY, M. & BRIOTTET. X. 1996. Selection and characterization of Saharan and Arabian Desert sites for the calibration of optical satellite sensors. *Remote Sensing of Environment, 58(1): 101-114.*

CURRAN, P. J. 1988. The semivariogram in remote sensing: An introduction. *Remote Sensing of Environment,* 24**,** 493-507.

DE VRIES, C., DANAHER, T., DENHAM, R., SCARTH, P. & PHINN, S. 2007. An operational radiometric calibration procedure for the Landsat sensors based on pseudo-invariant target sites. *Remote Sensing of Environment, 107, 414-429.*

EARL, R. A. 1990. Arid zone geomorphology. *edited by D. S. G. Thomas, Belhaven, London, 1989. No. of pages: 372. ISBN 0470 21341 8. Earth Surface Processes and Landforms, 15, 761-762.*

FOODY, G. M. 2001. GIS: the accuracy of spatial data revisited. *Progress in Geography, 389-93.*

FOODY, G. M. & ATKINSON, P. M. (eds.) 2002. *Uncertainty in Remote Sensing and GIS*: John Wiley and Sons Inc, USA.

FOX, N. 2001. Traceability to SI for EO measurements. . *CEOS WGCV Cal/Val Newsletter 9, January 2001, pp. 1-9, Available online at: http://wgcv.ceos.org/docs/newsletters/wgcv_newsletter_issue9.pdf (accessed 02 August 2010).*

FOX, N. 2009. A guide to expression of uncertainty of measurements GEO, Quality Assurance for Earth Observation Guide: 23rd May 2009,. *Available online at: http://qa4eo.org/docs/QA4EO-QAEO-GEN-DQK-006_v3.0.pdf (accessed 12 December 2010).*

GAO, F., SCHAAF, C. B., STRAHLER, A. H., JIN, Y. & LI, X. 2003. Detecting vegetation structure using a kernel-based BRDF model. *Remote Sensing of Environment, 86, 198-205*.

GOBRON, N., PINTY, B., AUSSEDAT, O., TABERNER, M., FABER, O., MÉLIN, F., LAVERGNE, T., ROBUSTELLI, M. & SNOEIJ, P. 2008. Uncertainty estimates for the FAPAR operational products derived from MERIS -- Impact of top-of-atmosphere radiance uncertainties and validation with field data. *Remote Sensing of Environment,* 112**,** 1871-1883.

GU, X. F., GUYOT, G. & VERBRUGGHE, M. 1992. Evaluation of measurement errors in ground surface reflectance for satellite calibration. *International Journal of Remote Sensing, 13(14): 2531-2546.*

GUOYONG, W., SI-CHEE, T., CAHALAN, R. F. & OREOPOULOS, L. 1999. Path radiance technique for retrieving aerosol optical thickness over land. *Journal of Geophysical Research, 104, 31321-32.*

GUROL, S., OZEN, H., LELOGLU, U. M. & TUNALI, E. 2008. Tuz Gölü: New Absolute Radiometric Calibration Site *The International Archives of the Photogrammetry, Remote Sensing and Spatial Information Sciences. Vol. XXXVII. Part B1. Beijing.*

KNEUBÜHLER, M., SCHAEPMAN, M. E. & THOME, K. J. 2006. Long - term Vicarious Calibration Efforts of MERIS at Railroad Valley Playa (NV) - An Update. *EARSeL and Warsaw University, Warsaw 2005. Proceedings of 4th EARSeL Workshop on Imaging Spectroscopy. New quality in environmental studies. Zagajewski B., Sobczak M., Wrzesień M., (Eds).*

KRIEBEL, K. T. 1976. On the Variability of the Reflected Radiation Field due to differing distributions of the irradiation. *Remote Sensing of Environment, 4, 257-264.*

KUUSK, A., KUUSK, J. & LANG, M. 2009. A dataset for the validation of reflectance models *Remote Sensing of Environment, 113, 889-92*.

LEDREW, E. & LIM, A. 2005. The application of the Getis statistic to high resolution imagery to detect change in the spatial structure of submerged tropical corals between image dates. *In: 2005 International Workshop on the Analysis of Multi-Temporal Remote Sensing Images, 16-18 May 2005, 2005 Piscataway, NJ, USA. IEEE, 217-19.*

LEDREW, E. F., HOLDEN, H., WULDER, M. A., DERKSEN, C. & NEWMAN, C. 2004. A spatial statistical operator applied to multidate satellite imagery for identification of coral reef stress *Remote Sensing of Environment, 91, 271-279.*

MAGEE, J. W. 1991. Late quaternary lacustrine, groundwater, aeolian and pedogenic gypsum in the Prungle Lakes, southeastern Australia. *Palaeogeography, Palaeoclimatology, Palaeoecology, 84, 3-42.*

MAIGNAN, F., BREON, F. M. & LACAZE, R. 2004. Bidirectional reflectance of Earth targets: Evaluation of analytical models using a large set of spaceborne measurements with emphasis on the Hot Spot. *Remote Sensing of Environment, 90, 210-220.*

MILTON, E. J., SCHAEPMAN, M. E., ANDERSON, K., KNEUBUHLER, M. & FOX, N. 2009. Progress in field spectroscopy. *Remote Sensing of Environment, 113, S92-S109.*

MIURA, T., HUETE, A. R. & YOSHIOKA, H. 2000. Evaluation of sensor calibration uncertainties on vegetation indices for MODIS. *Geoscience and Remote Sensing, IEEE Transactions on,* 38**,** 1399-1409.

MODIS DATA PRODUCT HANDBOOK 2009. *URL:www.pdaac.usgs.gov/lpdaac/products/modis_products_table/surface_reflectance/8_day_l3_global_500m/mod09a1 or http://modis.gsfc.nasa.gov/data/dataprod/pdf/MOD_09.pdf (Accessed on: 18th October, 2010).*

MORAN, M. S., BRYANT, R., HOLIFIELD, C. D. & MCELORY, S. 2003. Refined empirical line approach for retrieving surface reflectance from EO-1 ALI images *IEEE Transactions on Geoscience and Remote Sensing 41, 1411-1414.*

MORAN, M. S., BRYANT, R., THOME, K., NI, W., NOUVELLON, Y., GONZALEZ-DUGO, M. P., QI, J. & CLARKE, T. R. 2001. A refined empirical line approach for reflectance factor retrieval from Landsat-5 TM and Landsat-7 ETM+. *Remote Sensing of Environment, 78, 71-82.*

MUSTAFA, Y. & SOĞANCI, A. S. 2010. Evaluatuin of geotechnical properties of the salt layers on the Lake Tuz. *Scientific Research and Essays, Academic Journals. Vol. 5(18), pp. 2656–2663.*

NATIONAL PHYSICAL LABORATORY 2010. Measuring salt shine to improve climate understanding. *URL: http://www.npl.co.uk/news/measuring-salt-shine-to-improve-climate-understanding [Accessed on: 28/11/ 2010].*

NCAVEO 2005. *Calibration, NCAVEO,Chilbolton. URL:http://www.ncaveo.ac.uk/calibration/radiometry/in-flight/ [Accessed: 14/08/ 2010].*

NICODEMUS, F. E., RICHMOND, J. C., HSIA, J. J., GINSBERG, I. W. & LIMPERIS, T. 1977. Geometrical considerations and nomenclature for reflectance. *USA: Nat. Bur. Stand., Washington, DC, USA.*

ODONGO, V. 2010. *Uncertainity in reflectance factors measured in the field: Implications for the use of ground targets in remote sensing.* MSc Thesis, Twente University, Netherlands, pp86.

OLESON, K. W., BONAN, G. B., SCAAF, C., GAO, F., JIN, Y. & STRAHLER, A. 2003. Assessment of global climate model land surface albedo using MODIS data. *Geophysical Research Letters, 30, 26-1.*

PEGRUM, H. 2008. Tuz Gölü Salt Lake Test Site Characterisation Technical Report, Univesity of Southampton.

PINTY, B., LATTANZIO, A., MARTONCHIK, J. V., VERSTRAETE, M. M., GOBRON, N., TABERNER, M., WIDLOWSKI, J. L., DICKINSON, R.

E. & GOVAERTS, Y. 2005. Coupling diffuse sky radiation and surface albedo. *Journal of the Atmospheric Sciences, 62, 2580-91.*

RICHTER, R. 2007. Atmospheric/Topographic Correction for Satellite Imagery (ATCOR-2/3 User Guide, Version 6.3). *DLR- German Aerospace Centre, Remote Sensing Data Center, D – 82234 Wessling, Germany. DLR – IB 565- 01/07.*

RONDEAUX, G., STEVEN, M. D., CLARK, J. A. & MACKAY, G. 1998. La Crau: A European test site for remote sensing validation. . *International Journal of Remote Sensing, 19: 2775-2788.*

SCHAEPMAN-STRUB, G., SCHAEPMAN, M. E., PAINTER, T. H., DANGEL, S. & MARTONICHIK, J. V. 2006. Reflectance quantities in optical remote sensing-definitions and case studies. *Remote Sensing of Environment, 103, 27-42.*

SCOTT, K. P., THOME, K. J. & BROWNLEE, M. R. 1996. Evaluation of the Railroad Valley playa for use in vicarious calibration. *Proceedings of SPIE, vol. 2818, pp. 158-166. .*

SELLERS, P. J. 1995. Remote sensing of the land surface for studies of global change: models - algorithms - experiments. *Remote Sensing of Environment, 51, 3-26.*

SIX, D., FILY, M., ALVAIN, S., HENRY, P. & BENOIST, J. P. 2004. Surface Characterisation of the Dome Concordia Area (Antarctica) as a Potential Satellite Calibration Site, Using SPOT 4/VEGETATION Instrument. *Remote Sensing of Environment, 89: 83-94.*

SLATER, P. N., BIGGAR, S. F., HOLM, R. A., JACKSON, R. D., MAO, Y., MORAN, M. S., PALMER, J. M. & YUAN, B. 1987. Reflectance-and Radiance-Based Methods for In-Flight Absolute Calibration of Multispectral Sensors. *Remote Sensing of Environment, 22: 11-37.*

SPIKER, J. S. & WARMER, T. A. 2007. Scale and Spatial Autocorrelation From A Remote Sensing Perspective. *J. Scott Spiker Department of Geography, University of Wisconsin -Parkside, Kenosha, Wisconsin, Timothy A. Warner Department of Geology and Geography, West Virginia University, Morgantown, West Virginia.*
http://www.pelagicos.net/SpatialEcology/Readings/Spiker_Warmer_2007

TEILLET, P. M., FEDOSEJEVS, G. & GAUTHIER, R. P. 1998. Operational Radiometric Calibration of Broad scale Satellite Sensors Using Hyperspectral Airborne Remote Sensing of Prairie Rangeland: First Trials. *Metrologia, 35:639-641.*

TEILLET, P. M., FEDOSEJEVS, G., GAUTHIER, R. P., O'NEILL, N. T., THOME, K. J., BIGGAR, S. F., RIPLEY, H. & MEYGRET, A. 2001. A Generalized Approach to the Vicarious Calibration of Multiple Earth Observation Sensors Using Hyperspectral Data *Remote Sensing of Environment, 77(3): 304-327.*

TEILLET, P. M., FEDOSEJEVS, G., THOME, K. J. & BARKER, J. L. 2007. Impacts of spectral band difference effects on radiometric cross-calibration between satellite sensors in the solar-reflective spectral domain *Remote Sensing of Environment, in press. .*

TEILLET, P. M., SLATER, P. N., DING, Y., SANTER, R. P., JACKSON, R. D. & MORAN, M. S. 1990. Three Methods for the Absolute Calibration of the

NOAA AVHRR Sensors In-Flight. . *Remote Sensing of Environment, 31: 105-120.*

THE YALE CENTER FOR EARTH OBSERVATION 2010. *ULR: http://www.yale.edu/ceo. [Accessed : 16/10/2010].*

THOME, K. J. 2001. Paper on the ISPRS Commission I Mid-Term Symposium in conjunction with Pecora 15/Land Satellite Information IV Conference "Ground look radiometric calibration approaches for remote sensing imagers in the solar reflective". *Denver, CO USA. PDF.*

THOME, K. J. 2004. In-flight intersensor radiometric calibration using vicarious approaches. *Post-launch calibration of satellite sensors. Morain, S. A. and Budge, A. M. London, Taylor and Francis, 95-102.*

THOME, K. J., CROWTHER, B. G. & BIGGAR, S. F. 1997. Reflectance- and Irradiance-Based Calibration of Landsat-5 Thematic Mapper *Canadian Journal of Remote Sensing 23: 309-317.*

THOME, K. J., SCHILLER, S., CONEL, J., ARAI, K. & TSUCHIDA, S. 1998. Results of the 1996 Earth Observing System vicarious calibration joint campaign at Lunar Lake Playa. *Metrologia, 35: 631-638.*

WILSON, R. T. 2009. RTWTools for ENVI, Version 0.5, Available at http://rtwtools.googlecode.com.

WOODCOCK, C. E., STRAHLER, A. H. & JUPP, D. L. B. 1988. The use of variograms in remote sensing: II. Real digital images. *Remote Sensing of Environment,* 25**,** 349-379.

WULDER, M. & BOOTS, B. 1998. Local spatial autocorrelation characteristics of remotely sensed imagery assessed with the Getis statistic. *International Journal of Remote Sensing, 19, 2223-2231*

ZHANG, J. & GOODCHILD, M. 2002. Unicertainity in Geographical Information *(London: Taylor and Francis).*

9. APPENDICES

Appendix 1: *Description of Parameters entered in ATCOR-2^{TM} Software during the radiometric and atmospheric correction of the Landsat TM and ASTER datasets*

Parameters	Description and Entry value
"Atm. Correction" type	"ATCOR2: multispectral sensors, flat terrain" option was selected. This option was chosen due to the terrain type of the study site (Tuz Gölü) being flat where no digital elevation model required and the satellite sensor type.
Date (*dd/mm/yyyy*)	Provide date with regarding the day, month (*mm*) and year (*yyyy*) the input satellite data was acquired. E.g. for LTM19840824.bsq (i.e. *dd* = 24, *mm* = 08 and *yyyy* = 1984) (see table 2).
Input image file	The image file to be ATCOR'ed is selected. E.g.LTM19840824.bsq (i.e. Landsat image acquired on 24th August, 1984). The input image should have a band sequential format (bsq) which is appropriate and compatible with ATCOR software.
Output image file	Provide name for the output ATCOR'ed image E.g.LTM19840824_*atm*.bsq (where: _*atm* represents the ATCOR'ed file and useful in differentiating the ATCOR'ed file from the other output files produced during the ATCOR process).

Scale Factor	Provide information on the multiplication factor for the surface reflectance recognized in the output image file. This ranges from 0 – 100%. A scale factor of 4 was selected since the input datasets were 8 bits. This implies that a surface reflectance of 20% will be coded as 80.
Selected Sensor	Based on the satellite image under investigation (LTM19840824.bsq), the right sensor type (in this case Landsat TM 4/5) was selected. This step automatically specifies the recommended values for the Sensor's View Geometry, Band Selection, Spatial Sub-image and Pixel size parameters. However, these parameters can be manually altered.
Calibration File	The Calibration File contains information responsible for the radiometric and atmospheric correction process. This file is sensor specific. Thus, in this study, standard Landsat calibration file and ASTER calibration file were chosen for the Landsat and ASTER images under investigation respectively.
Atmospheric File	This file centres on the VNIR and SWIR bands and contains the look-up table (LUT) results of the radiative transfer calculations. The selection of Atmospheric File is based on the geographic location of the site (i.e. rural, urban and desert) and the period of the year (mid latitude summer, winter and fall). Thus, in this study, the rural mid latitude summer, winter and fall files selected for July/August, April and October images respectively.

Atmospheric File for Thermal bands	This file centres on the thermal bands. The selection of Atmospheric File for the thermal bands was based on the geographic location of the site (i.e. rural, urban and desert) and the period of the year (mid latitude summer, winter and fall). Thus, in this study, the rural mid latitude summer, winter and fall files selected for July, April and October ASTER images respectively.
Adjacency range	The adjacency range was set to 1km and Zone was set to 1.
Solar Zenith Angle	The values of the Solar Zenith Angles (SZA) entered for the images were retrieved from their metadata files respectively. The SZA was estimated by subtracting the Sun Elevation Angle value of each image from $90°$ (see appendix).
Ground Elevation	The Ground Elevation is the value of the altitude of the area/site under investigation. Thus, a value of 905km was entered for all the images, which is the altitude of Tuz Gölü.
Visibility (km)	The visibility values used were automatically determined after exploiting the "VISIB. ESTIMATE", "SPECTRA" and "AEROSOL TYPE" options which are used to assessing the quality of the atmospheric correction prior to processing the image date.

Appendix 2: *Description of the ASTER Bands*

Band	Label	Wavelength (µm)	Resolution
B1	VNIR_Band1	0.52 - 0.60	15m
B2	VNIR_Band2	0.63 - 0.69	15m
B3	VNIR_Band3N	0.76 - 0.86	15m - Nadir view
B4 scan	VNIR_Band3B	0.76 - 0.86	15m - Backward

(Used to create high resolution DEM)

SWIR data invalid as of April 2008

Band	Label	Wavelength (µm)	Resolution
B5	SWIR_Band4	1.60 - 1.70	30 m
B6	SWIR_Band5	2.145 - 2.185	30 m
B7	SWIR_Band6	2.185 - 2.225	30 m
B8	SWIR_Band7	2.235 - 2.285	30 m
B9	SWIR_Band8	2.295 - 2.365	30 m
B10	SWIR_Band9	2.36 - 2.43	30 m
B11	TIR_Band10	8.125 - 8.475	90m
B12	TIR_Band11	8.475 - 8.825	90m
B13	TIR_Band12	8.925 - 9.275	90m
B14	TIR_Band13	10.25 - 10.95	90m
B15	TIR_Band14	10.95 - 11.65	90m

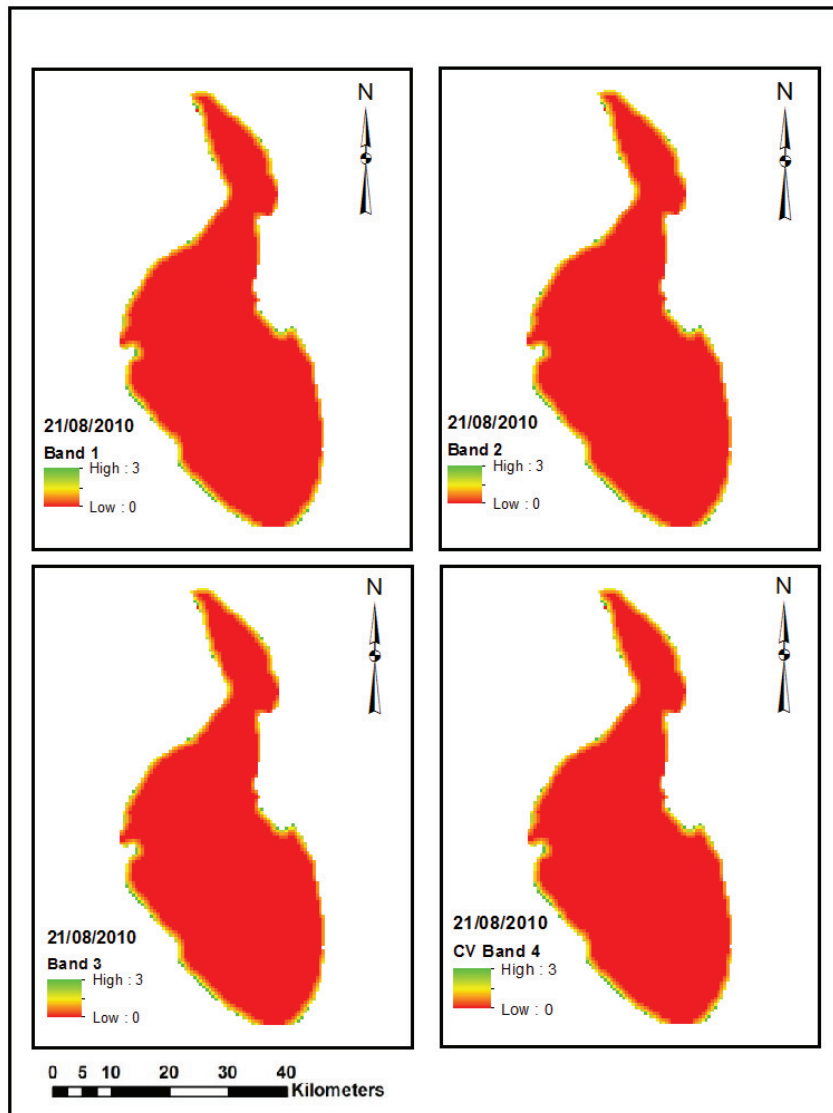Source: Adapted from http://www.yale.edu/ceo

Appendix 3: CV index map of Tuz Gölü showing MODIS TERRA (MOD09A1) band 1, 2, 3 & 4 at 480m pixel resolution for the month of July 2010
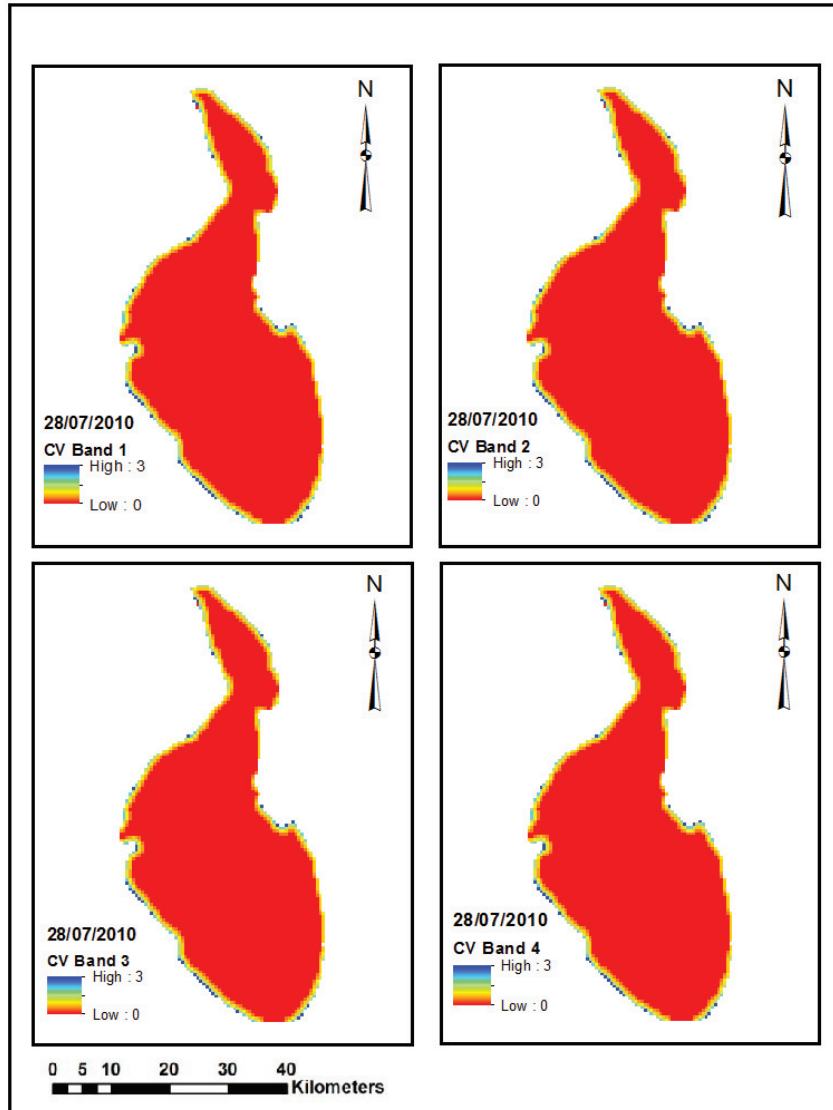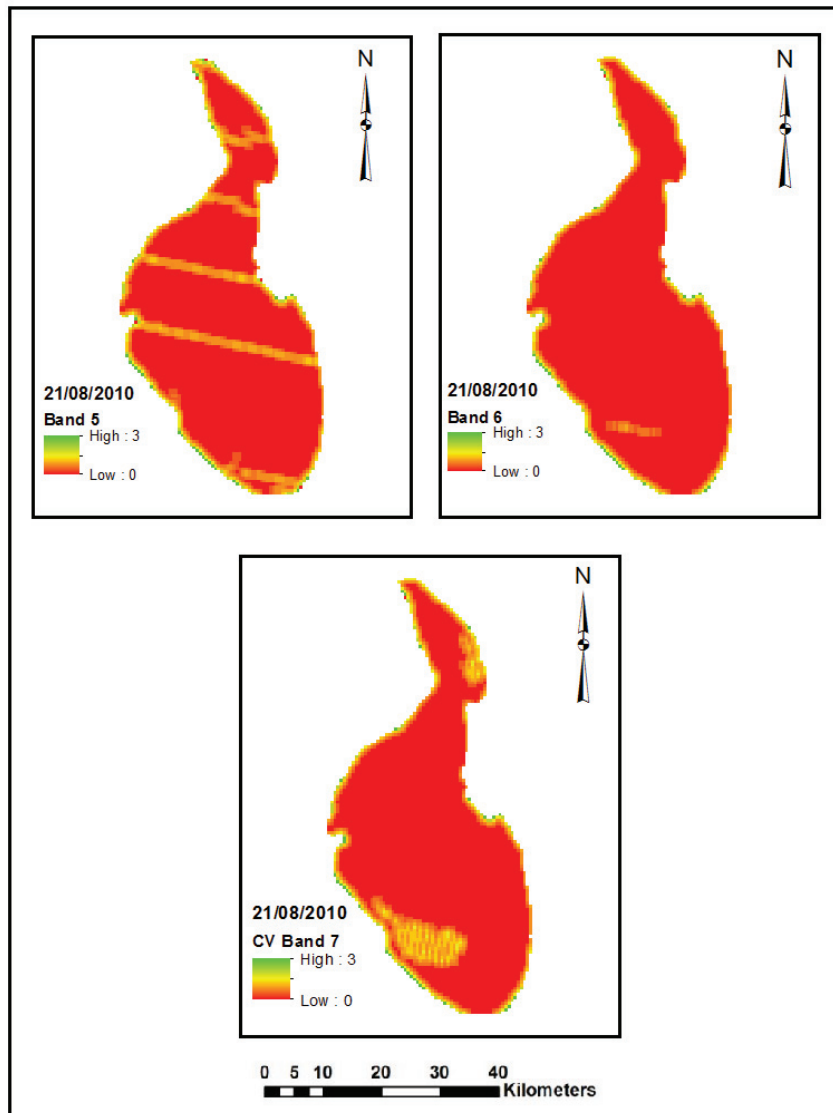
Appendix 4: CV index map of Tuz Gölü showing MODIS TERRA (MOD09A1) band 5, 6 & 7 at 480m pixel resolution for the month of July 2010
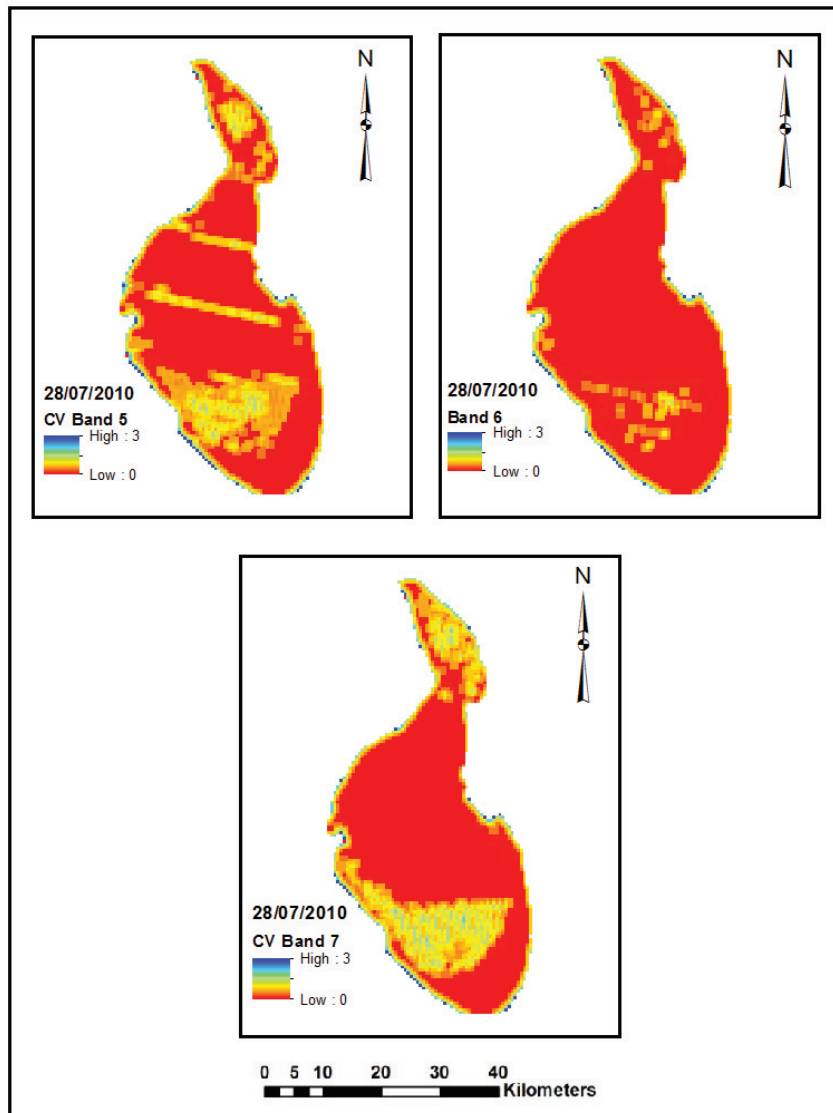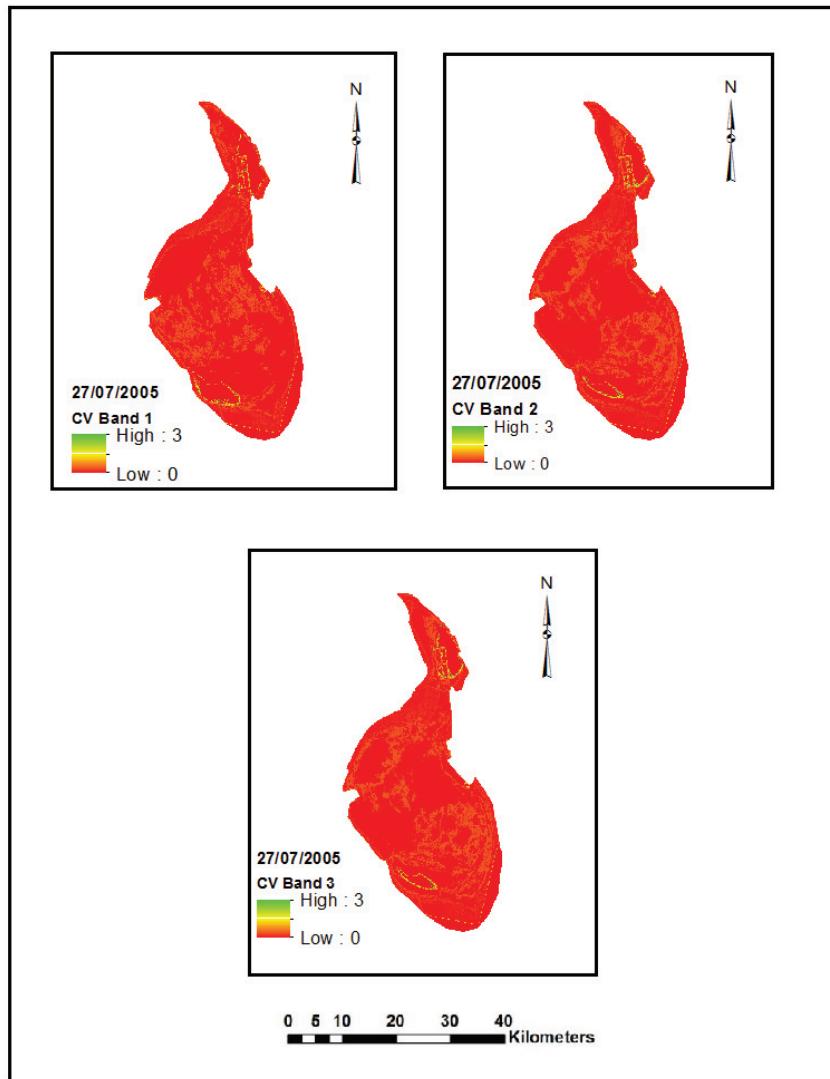
Appendix 5: CV index map of Tuz Gölü showing MODIS TERRA (MOD09A1) band 1, 2, 3 & 4 at 480m pixel resolution for the month of August 2010

Appendix 6: CV index map of Tuz Gölü showing MODIS TERRA (MOD09A1 band 5, 6 & 7 at 480m pixel resolution for the month of August 2010
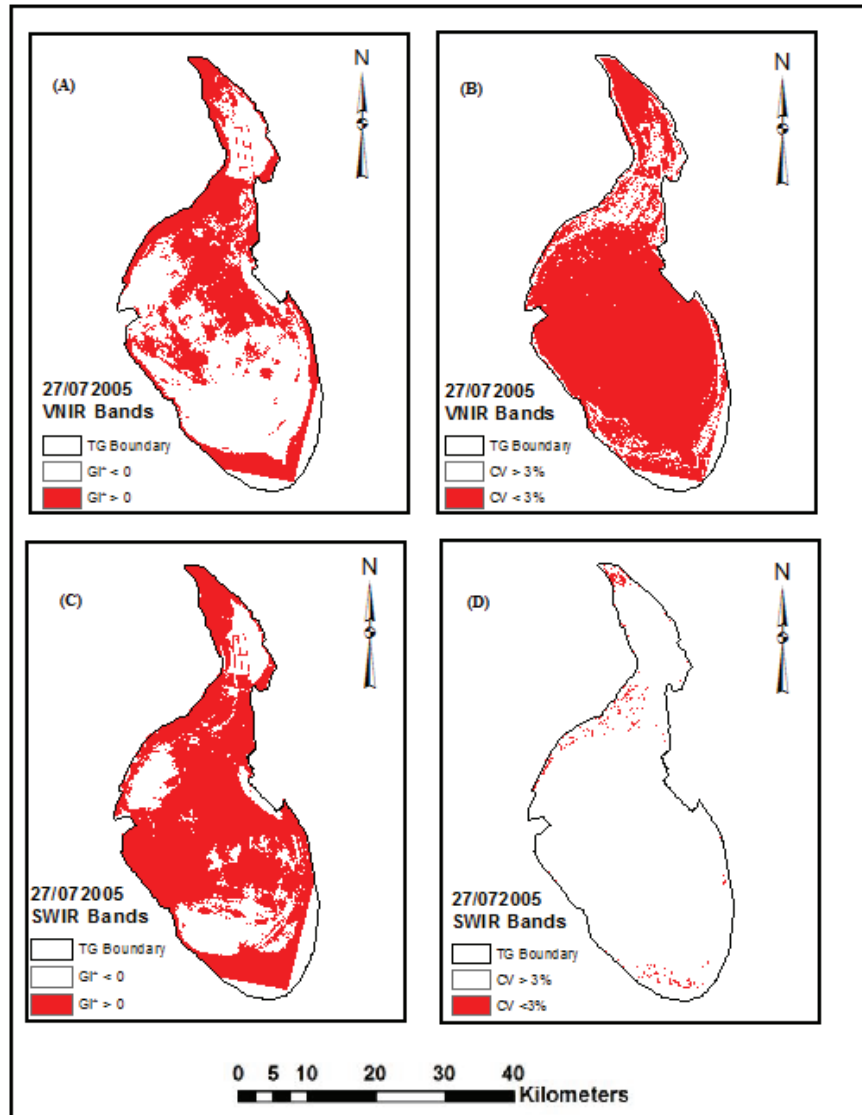
Appendix 7: CV index map of Tuz Gölü showing ASTER VNIR bands at 30 m pixel resolution for the month of July 2005.
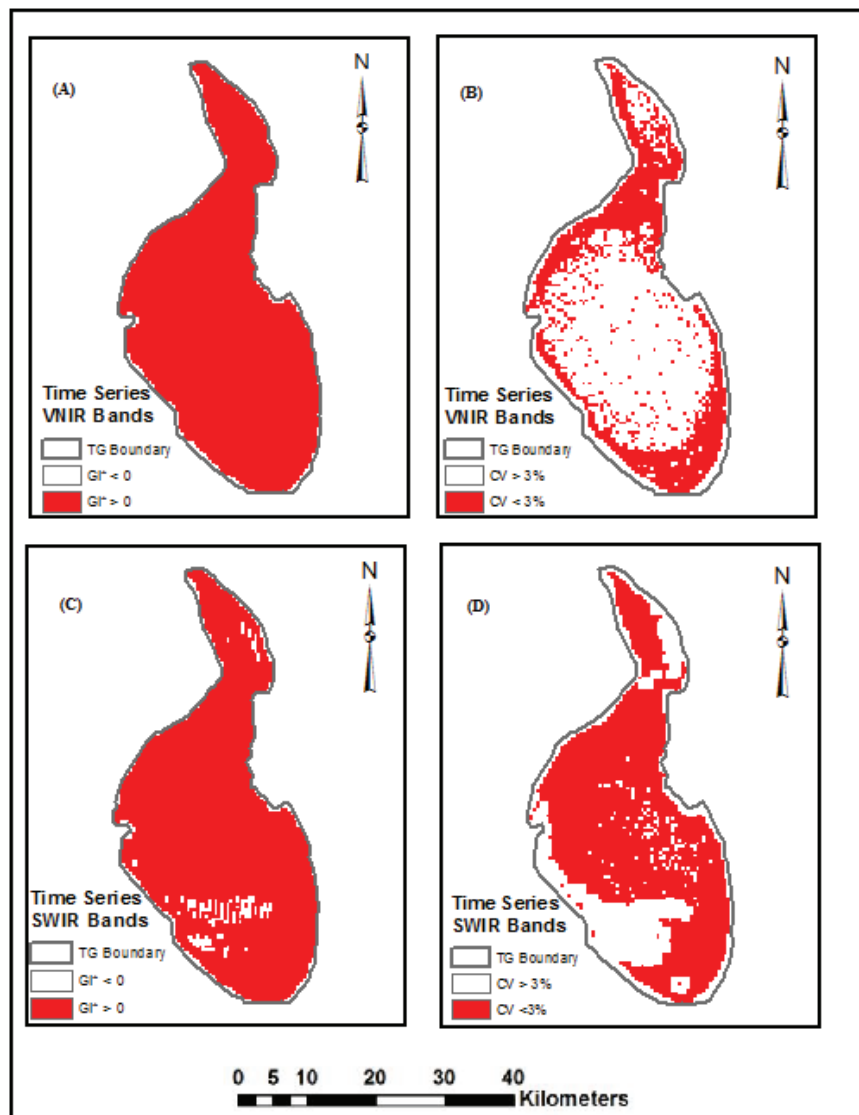
Appendix 8: CV (CV < 3%) and Getis (Gi*> 0) index maps of Tuz Gölü showing ASTER L1B VNIR [(A) & (B)] and SWIR [(C) & (D)] bands at 30 m pixel resolution for the month July, 2005.

Appendix 9: Time Series CV (CV < 3%) and Getis (Gi*> 0) index maps of Tuz Gölü showing MODIS (MOD09A1) VNIR [(A) & (B)] and SWIR [(C) & (D)] bands at 480m pixel resolution for the month August comprising of years 2004, 2005 and 2006.

Appendix 10: (a) Spatial homogeneity index map of TG based on Landsat TM for the month of August for 1984, 1989 (2 images), 1998, 2000, 2003, 2006, 2009 (3 images) integrating bands 1, 2, 3, 4 (adopted) from Odongo, 2010) (b) Spatial homogeneity index map of NPL based on MODIS (LPDAAC, 2007) satellite images of July and August (2004-2006) for using only red and near infra-red bands (Adopted from Pegrum, 2008).
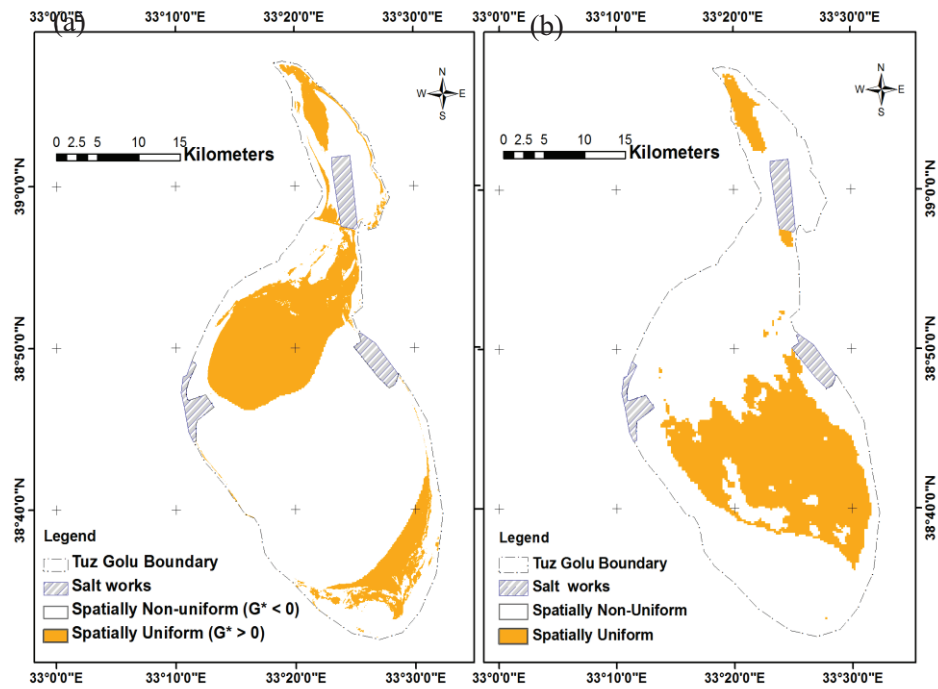
Source: Odongo (2010)

Appendix 11: CV index map of Tuz Gölü showing ASTER SWIR bands at 30 m pixel resolution for the month of July 2005
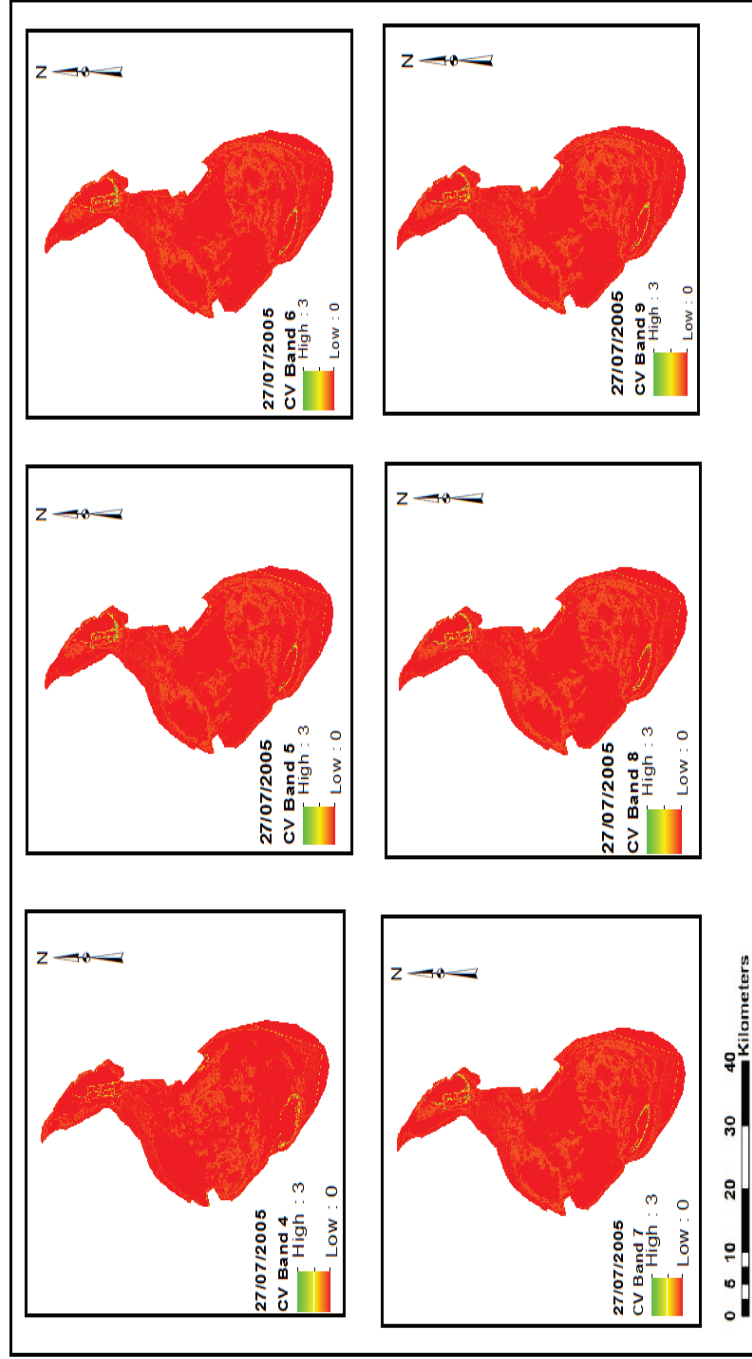
Appendix 12: CV index map of Tuz Gölü showing Landsat TM VNIR and SWIR bands at 30 m pixel resolution for the month of August 2010